# Height models on a honeycomb lattice

Masterarbeit
der Philosophisch-naturwissenschaftlichen Fakultät
der Universität Bern

vorgelegt von
**Bühlmann Patrick**

**2018**

Leiter der Arbeit
**Prof. Dr. Uwe-Jens Wiese**

Albert Einstein Center for Fundamental Physics
Institute for Theoretical Physics
University of Bern

## Abstract

In this thesis we study a two-dimensional constrained height model on a honeycomb lattice, motivated by a lecture given by Prof. M. Hairer in 2016 at the University of Bern. This model has a one-to-one correspondence to an $F$ Model on a triangular lattice. By using a multi-cluster algorithm, we simulate this model and obtain a dual form of a Berezinsky-Kosterlitz-Thouless phase transition which is being investigated.

# Contents

# 1 Introduction

Historically, research in physics was carried out by experiments or by theoretical investigations. With the invention of computers, it became possible to carry out simulations of theoretical models, i.e. physicists were not only able to construct theoretical models for analytical investigations, but have also been able to solve them numerically. Since computer power has increased drastically and efficient simulation algorithms have been constructed, computational physics has become an important branch of physics, thus computer simulations have become an accepted method of scientific research.

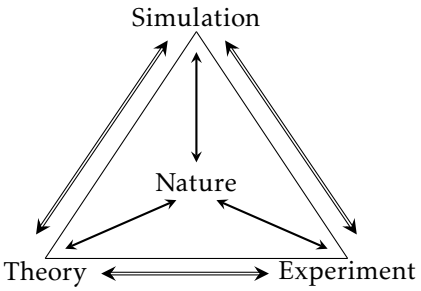


**Figure 1.1:** Schematic view of the relationship between theory, experiment, and simulations.

In this thesis we use simulations in order to investigate a constrained height model that was mentioned by Prof. M. Hairer in 2016 at his Einstein lectures in Bern. Throughout this thesis we refer to this model as the $\tilde{F}_\Delta$ model, motivated by the one-to-one correspondence to the $F$ model on a triangular lattice (which we label the $F_\Delta$ model). Both models are related to each other by duality. The $\tilde{F}_\Delta$ model, a two-dimensional lattice model on a honeycomb lattice, is defined to have an integer-valued height variable (or spin variable) on each site of the honeycomb lattice and nearest-neighbors are constrained to a height difference of $\pm 1$. Those height variables can be thought of as a height of a surface above the two-dimensional lattice. We refer to this surface as a height field. Due to the constraint we impose, the height field is smooth in the sense that the difference between neighboring height variables is not bigger than 1. Furthermore, the constraint implies that next-nearest-neighbors can have a height differences of 0 or $\pm 2$, where the $\pm 2$ bonds are assigned a smaller Boltzmann weight.
A similar model on a square lattice has been investigated [1] and a roughening transition was found, separating a rigid (smooth) phase from a rough one. The $\tilde{F}_\Delta$ model also undergoes a phase transition, a dual form of the Berezinsky-Kosterlitz-Thouless phase transition, which we are going to investigate. In Chapter 2 and 3 we provide basic knowledge about classical statistical mechanics and Monte Carlo simulations. We set the framework in Chapter 4 by introducing the honeycomb lattice and in Chapter 5 we define the $\tilde{F}_\Delta$ model in terms of a partition function. Furthermore, we are going to establish the duality between the $F_\Delta$ model and the $\tilde{F}_\Delta$ model. In Chapter 6 we describe the algorithm which is used in order to simulate the $\tilde{F}_\Delta$ model and we discuss some interesting variables. The results being discussed in Chapter 7 and 8.

# 2 Classical Statistical Mechanics

In this section basic features of classical statistical mechanics, with a focus on spin systems are being reviewed. The interested reader is referred to [2, 3] for a more detailed discussion.

## 2.1 Partition Function

Statistical mechanics is based upon the idea of a partition function which describes the statistical properties of a system in thermodynamical equilibrium. For a classical statistical system the canonical partition function is given by

$$Z(\beta) = \sum_{[\mathrm{s}]} e^{-\beta \mathcal{H}[\mathrm{s}]}, \tag{2.1}$$

where $\mathcal{H}[\mathrm{s}]$ is the Hamiltonian as a functional of a given spin configuration [s] and $\beta = \frac{1}{k_B T}$. The variable $T$ denotes the temperature, $k_B$ is the Boltzmann constant, and the summation extends over all possible spin configurations. One defines observables as

$$\langle \mathcal{O} \rangle = \sum_{[\mathrm{s}]} p[\mathrm{s}] \mathcal{O}[\mathrm{s}], \tag{2.2}$$

where $\mathcal{O}[\mathrm{s}]$ denotes the measured quantity of the configuration [s] and $p[\mathrm{s}]$ denotes the probability of the system to be in a particular configuration [s] given by

$$p[\mathrm{s}] = \frac{1}{Z(\beta)} e^{-\beta \mathcal{H}[\mathrm{s}]}. \tag{2.3}$$

## 2.2 Classical Spin Models

One distinguishes continuous and discrete spin models, depending on whether the spins take their values in a continuous or discrete target space. Spin models can also be characterized by their lattice geometry and their dimensionality $d$. Throughout this thesis we only consider the two-dimensional case $d = 2$. Usually, when defining Hamiltonians of spin systems one adds a contribution in form of an external magnetic field $h$. In this thesis, however, we define all Hamiltonians in the absence of symmetry breaking external fields. In 1952 Potts described a class of spin models [4] which are named after him, the standard $q$-state Potts model and the $q$-state clock model (which is also referred to as a $\mathbb{Z}_q$-model or $q$-state planar Potts model).
Both models impose a nearest-neighbor interaction and respect a $q$-periodicity ($q \in \mathbb{N}$) such that each spin variable can be parametrized by an integer-valued variable $n \in \{0, 1, \cdots, q-1\}$. The Boltzmann weight $u(n_x, n_y)$ for nearest-neighboring spins is a function of the difference only and it is periodic with period $q$, such that

$$u(n_x, n_y) = u(n_y - n_x) = u(n_y - n_x \mod q). \tag{2.4}$$

For our discussion the $q$-state clock model is of particular interest.

### 2.2.1 Clock Model

For the $q$-state clock model one attaches a 2-component unit-vector to each lattice site $x$, such that

$$\vec{e}_x = (\cos(\varphi_x), \sin(\varphi_x)). \tag{2.5}$$

This unit-vector at lattice site $x$ is parametrized by a discretized angle

$$\varphi_x = \frac{2\pi n_x}{q}, n_x \in \{0, 1, \cdots, q-1\}, \tag{2.6}$$

such that the vector is pointing towards the corners of a planar $q$-gon. The $q$-state clock model is characterized by the energy function

$$\mathcal{H}_{\text{clock}}[\varphi] = -J \sum_{\langle x,y \rangle} \vec{e}_x . \vec{e}_y = -J \sum_{\langle x,y \rangle} \cos(\varphi_y - \varphi_x), \tag{2.7}$$

where $\langle x, y \rangle$ indicates a summation over nearest-neighbors. Hence the partition function reads

$$Z_{\text{clock}}(\beta) = \sum_{[\varphi]} e^{-\beta \mathcal{H}_{\text{clock}}[\varphi]} = \left( \prod_x \sum_{\varphi_x \in \frac{2\pi}{q} \cdot \mathbb{Z}_q} \right) e^{-\beta \mathcal{H}_{\text{clock}}[\varphi]} = \left( \prod_x \sum_{n_x=0}^{q-1} \right) e^{-\beta \mathcal{H}_{\text{clock}}[\varphi]}. \tag{2.8}$$

Since the interaction only depends on spin differences it is invariant under global $\mathbb{Z}_q$-transformations

$$\varphi_x \mapsto \varphi_x + \frac{2\pi n}{q}, n \in \mathbb{Z}, \forall x. \tag{2.9}$$

For the case where $q = 2$ the energy of a single bond is $\pm J$, depending on whether the adjacent spins have the same value or not. Thus the case where $q = 2$ and $J > 0$ is equivalent to an Ising ferromagnet, if we consider integer-valued spins $s_x \in \{\pm 1\}$ and modify the Hamiltonian

$$\mathcal{H}_{\text{Ising}}[s] = -J \sum_{\langle x,y \rangle} s_x s_y. \tag{2.10}$$

We are going to use the Ising ferromagnet as a prime example throughout this thesis, in order to illustrate certain theoretical concepts.

### 2.2.2 U(1) Model and the XY Model

The $U(1)$ model can be obtained from the $q$-state clock model in the limit of infinite $q$. In this limit the angles $\varphi_x$ can take any value between 0 and $2\pi$, such that a spin is parametrized by an angle on a unit circle $S^1$. As the name suggests, this model has a global $U(1)$ symmetry, which means that the Hamiltonian stays invariant under a global angular valued transformation by a fixed angle $\hat{\varphi}$

$$\varphi_x \mapsto \varphi_x + \hat{\varphi}, \hat{\varphi} \in [0, 2\pi), \forall x. \tag{2.11}$$

The two-dimensional $U(1)$ model, which is known as the XY model, shows an unusual phase transition of infinite order, which is known as a Berezinsky-Kosterlitz-Thouless phase transition (see Subsection 2.6.5). In order to define the XY model, consider a two-dimensional lattice where each site carries a unit-vector as in Equation (2.5), parametrized by a continuous angle $\varphi \in [0, 2\pi)$. Angular differences are defined to be

$$\Delta\varphi_{xy} = \varphi_y - \varphi_x \mod 2\pi, \Delta\varphi_{xy} \in [0, 2\pi), \tag{2.12}$$

and the Hamiltonian is the same as for the $q$-state clock model

$$\mathcal{H}_{\text{XY}}[\varphi] = -J \sum_{\langle x,y \rangle} \cos(\varphi_y - \varphi_x). \tag{2.13}$$

Since configurations $[\varphi]$ are now described by continuous angular variables the summation in the partition function of the clock model is now replaced by an integration. Therefore we obtain for the XY model

$$Z_{\text{XY}}(\beta) = \left( \int \mathcal{D}\varphi \right) e^{-\beta \mathcal{H}_{\text{XY}}[\varphi]} = \left( \prod_x \int_0^{2\pi} \mathrm{d}\varphi_x \right) e^{-\beta \mathcal{H}_{\text{XY}}[\varphi]}. \tag{2.14}$$

### 2.2.3 Height Model

Consider a spin model where each lattice site $x$ is inhabited by an integer-valued spin variable $h_x \in \mathbb{Z}$. In this case the spins are interpreted as height variables. The difference of heights $h_y - h_x$ for adjacent lattice points $x$ and $y$ is related to the Hamiltonian $\mathcal{H}[\mathrm{h}]$. Consider for example the Hamiltonian

$$\mathcal{H}[\mathrm{h}] = \frac{J}{4} \sum_{\langle x,y \rangle} (h_y - h_x)^2, \tag{2.15}$$

where $J > 0$ and we have integer-valued height variables $h_x \in \mathbb{Z}$. We see that in the limit where the temperature $T$ goes to 0, flat height fields have a higher Boltzmann weight, whereas for high temperatures fluctuating height fields are more dominant in the partition function. Throughout this thesis, flat height fields, where fluctuations between neighboring height variables are minimized, are considered smooth height fields. They are characteristic for the rigid (smooth) phase, whereas fluctuating height fields are characteristic for the rough phase. Allowing the heights to be integer-valued is problematic because the partition function is not well-defined anymore. Any Hamiltonian depending on height differences is invariant under global shifts $h_x \mapsto h_x + n$, for any $n \in \mathbb{Z}$, which means that we have an infinite number of configurations. One can get rid of the global $\mathbb{Z}$ symmetry by fixing one height variable and imposing constraints which only allow for a finite number of configurations.

## 2.3 Dualization Relations among these Models

The previously presented lattice models are related to each other by duality transformations. A discussion of duality transformations and their geometrical interpretation for the honeycomb lattice is given in Chapter 4, and a detailed transformation for the $\tilde{F}_\Delta$ model is given in Chapter 5. A duality transformation maps a system of low temperature to a system of high temperature (and vice versa) and leads to new insights into critical regimes of the model. For a simple case like the Ising model, one can also say that an ordered phase (at low temperature) is mapped to a disordered phase (at high temperature) and vice versa. In the case where two lattice models are identical up to a rescaling of the Boltzmann weights we call a model self-dual. The dual transformation was first introduced for the Ising model on a square lattice by Kramers and Wannier in 1941 [5], in 1945 the dual lattice was introduced by Wannier giving a topological picture of the dual transformation [6]. Throughout this thesis the variables $x, y$ denote coordinates of the original lattice and variables with a tilde like $\tilde{x}, \tilde{y}$ denote coordinates of the dual lattice.

### 2.3.1 Dualization of the Clock Model on a Square Lattice

Consider the zero field $q$-state clock model on a square lattice, with Hamiltonian $\mathcal{H}_{\mathrm{clock}}[\varphi]$, given in Equation (2.7). The Boltzmann weights factorize such that the partition function can be written as

$$Z(\beta) = \sum_{[\varphi]} e^{-\beta \mathcal{H}[\varphi]} = \sum_{[\varphi]} \prod_{\langle x,y \rangle} u(n_y - n_x). \tag{2.16}$$

where $u(n_y - n_x)$ is the $q$-periodic Boltzmann factor. For the sake of simplicity we introduce a dimensionless coupling parameter

$$K = \beta J, \tag{2.17}$$

such that the partition function $Z$ is a function of $K$ ($Z = Z(K)$) and

$$u(n_y - n_x) = e^{K \cos(\frac{2\pi}{q}(n_y - n_x))}. \tag{2.18}$$

We assume that the square lattice has $N$ sites and we impose open boundary conditions. In order to dualize this model we need to impose an orientation on the bonds of the square lattice, indicating how we measure spin differences. We determine spin differences by the sense of arrows pointing up and right (see Figure 2.1). Duality of the partition function is derived by using the Fourier

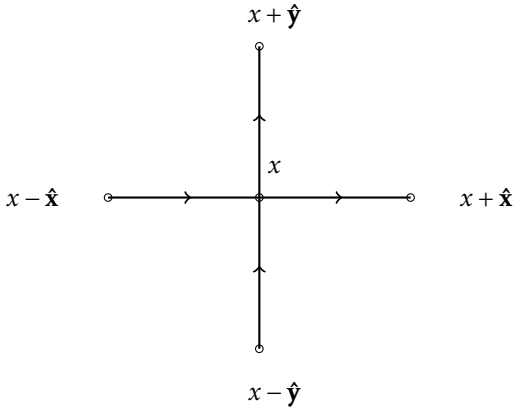


**Figure 2.1:** Definition of spin differences determined by the sense of arrows. The unit-vectors along the x and y axes are labeled $\hat{\mathbf{x}}$ and $\hat{\mathbf{y}}$.

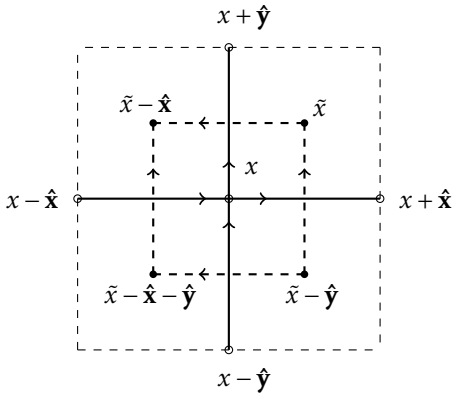


**Figure 2.2:** New spin variables $\tilde{n}_{\tilde{x}}$ introduced on the dual lattice. Coordinates of the dual lattice are denoted by a tilde, such as $\tilde{x}$.

transformation of the Boltzmann factor at each bond, such that

$$u(n_y - n_x) = \frac{1}{q}\sum_{k_{xy}=0}^{q-1} \exp\left(\frac{2\pi i}{q}(n_y - n_x)k_{xy}\right)\lambda(k_{xy}). \tag{2.19}$$

Now the dependence on $n_x$ is very simple and we can evaluate the partition function for this case. Plugging in Equation (2.19) we obtain

$$Z(K) = \sum_{[\varphi]}\prod_{\langle x,y\rangle} u(n_y - n_x) = \sum_{[\varphi]}\prod_{\langle x,y\rangle}\left(\frac{1}{q}\sum_{k_{xy}=0}^{q-1} e^{\frac{2\pi i}{q}(n_y-n_x)k_{xy}}\lambda(k_{xy})\right) \tag{2.20}$$

$$= (\frac{1}{q})^{2N}\left(\prod_{\langle x,y\rangle}\sum_{k_{xy}=0}^{q-1}\lambda(k_{xy})\right)\left(\prod_{x}\sum_{n_x=0}^{q-1}\prod_{\langle x,y\rangle} e^{\frac{2\pi i}{q}(n_y-n_x)k_{xy}}\right). \tag{2.21}$$

The case of the square lattice implies that for a given $x$, the variable $n_x$ appears in the Boltzmann factor for interactions with four neighboring sites. According to the way we defined spin differences, with the sense of arrows as up and right, we assign the sign such that $x$ is at the head of an arrow and $y$ is the tail in $n_x - n_y$. Then the summation over one site $x$ is of the form

$$\sum_{n_x=0}^{q-1}\exp\left(\frac{2\pi i}{q}\left((n_{x+\hat{\mathbf{x}}}-n_x)k_{x,x+\hat{\mathbf{x}}} + (n_x - n_{x-\hat{\mathbf{x}}})k_{x-\hat{\mathbf{x}},x} + (n_{x+\hat{\mathbf{y}}}-n_x)k_{x,x+\hat{\mathbf{y}}} + (n_x - n_{x-\hat{\mathbf{y}}})k_{x-\hat{\mathbf{y}},x}\right)\right). \tag{2.22}$$

Evaluating the sum over $n_x$ yields the constraint

$$k_{x,x+\hat{\mathbf{x}}} - k_{x-\hat{\mathbf{x}},x} + k_{x,x+\hat{\mathbf{y}}} - k_{x-\hat{\mathbf{y}},x} \mod q = 0, \tag{2.23}$$

for all lattice sites. The variables $k_{xy}$ act as bond variables between the spins. If we consider $k_{xy}$ as a current flowing along the bond $\langle x, y\rangle$, Equation (2.23) suggests that the current is conserved at each

site and thus the field is free of divergence. The partition function then takes the form

$$Z(K) = q^{N-2N} \sum_{[k_{xy}]}^{*} \prod_{\langle x,y \rangle} \lambda(k_{xy}), \tag{2.24}$$

where $\sum^{*}_{[k_{xy}]}$ denotes the sum over all bond configurations satisfying the constraint. The factor $q^{-2N}$ is a result of the $2N$ bonds and the definition of the discrete Fourier transformation. Assuming that all constraints are satisfied, the factor $q^N$ comes out after summing over all bond variables $k_{xy}$. The next step is to find a change of variables such that the constraints are satisfied. These variables are considered dual variables living on the dual lattice (see Figure 2.2). We first rotate the original bonds $k_{xy}$ consistently by an angle of 90 degrees and impose new variables $\tilde{n}$ at the tail of the arrows and at the head of the arrows. Define the new variables to be

$$k_{x,x+\hat{\mathbf{x}}} = \tilde{n}_{\tilde{x}} - \tilde{n}_{\tilde{x}-\hat{\mathbf{y}}}, \qquad k_{x,x+\hat{\mathbf{y}}} = \tilde{n}_{\tilde{x}-\hat{\mathbf{x}}} - \tilde{n}_{\tilde{x}}, \tag{2.25}$$

$$k_{x-\hat{\mathbf{x}},x} = \tilde{n}_{\tilde{x}-\hat{\mathbf{x}}} - \tilde{n}_{\tilde{x}-\hat{\mathbf{x}}-\hat{\mathbf{y}}}, \qquad k_{x-\hat{\mathbf{y}},x} = \tilde{n}_{\tilde{x}-\hat{\mathbf{x}}-\hat{\mathbf{y}}} - \tilde{n}_{\tilde{x}-\hat{\mathbf{y}}}, \tag{2.26}$$

all of which are modulo $q$, and we introduced dual coordinates $\tilde{x}$ on the dual lattice. Using this change of variables the constraint is satisfied and we end up with the dual partition function given by

$$Z(K) = \left(\frac{1}{q}\right)^N \sum_{[\tilde{n}]} \prod_{\langle \tilde{x},\tilde{y} \rangle} \lambda(\tilde{n}_{\tilde{y}} - \tilde{n}_{\tilde{x}}) = (\frac{1}{q})^N \tilde{Z}(\tilde{K}), \tag{2.27}$$

where $\tilde{K}$ denotes the dual partition function with some dual coupling parameter $\tilde{K}$. The Boltzmann weight $\lambda$ for the dual partition function $\tilde{Z}$ reads

$$\begin{aligned} \lambda(\tilde{n}_{\tilde{y}} - \tilde{n}_{\tilde{x}}) &= \sum_{k_{xy}=0}^{q-1} \exp\left(\frac{-2\pi i}{q}(\tilde{n}_{\tilde{y}} - \tilde{n}_{\tilde{x}})k_{xy}\right) u(k_{xy}) \\ &= \sum_{k_{xy}=0}^{q-1} \exp\left(-i(\frac{2\pi\tilde{n}_{\tilde{y}}}{q} - \frac{2\pi\tilde{n}_{\tilde{x}}}{q})k_{xy} + K\cos(\frac{2\pi k_{xy}}{q})\right). \end{aligned} \tag{2.28}$$

The dual Boltzmann weight $\lambda$ is $q$-periodic, has its maximum at $\lambda(0)$ and its minimum at $\lambda(q/2)$ for $q$ even or $\lambda((q+1)/2)$,$\lambda((q-1)/2)$ for $q$ odd. These are the same characteristics the original Boltzmann weight $u$ has, therefore $\lambda$ describes the same physics and the model is self-dual. Ideally we want to relate the dual Boltzmann weight $\lambda = \lambda(\tilde{n}_{\tilde{y}} - \tilde{n}_{\tilde{x}})$, with its dual coupling parameter $\tilde{K}$ such that

$$\lambda(\tilde{n}_{\tilde{y}} - \tilde{n}_{\tilde{x}}) \propto e^{\tilde{K}\cos(\frac{2\pi}{q}(\tilde{n}_{\tilde{y}} - \tilde{n}_{\tilde{x}}))}. \tag{2.29}$$

Using this identification one tries to deduce a duality relation between $K$ and $\tilde{K}$ such that we can associate a weak coupling phase in $K$ with a strong coupling phase in $\tilde{K}$ and vice versa. For general $q$ such a relation is difficult to deduce analytically, but for the case $q = 2$ (Ising model) it can be accomplished. For $q = 2$ we have $u(0) = e^K$, $u(1) = e^{-K}$ in the original model. The Boltzmann weights of the dual model then read $\lambda(0) = e^K + e^{-K}$ and $\lambda(1) = e^K - e^{-K}$. Since the ratio of Boltzmann factors for the two states of neighboring spins is $u(1)/u(0) = e^{-2K}$, it is reasonable to define $\lambda(1)/\lambda(0) = e^{-2\tilde{K}}$, such that the duality between the two couplings reads

$$e^{-2\tilde{K}} = \tanh(K) \leftrightarrow (e^{2K} - 1)(e^{2\tilde{K}} - 1) = 2. \tag{2.30}$$

The dual Boltzmann weight $\lambda$ is now given by

$$\lambda(\tilde{n}_{\tilde{y}} - \tilde{n}_{\tilde{x}}) = e^{\tilde{K}\cos(\pi(\tilde{n}_{\tilde{y}} - \tilde{n}_{\tilde{x}}))+a}, \tag{2.31}$$

where the constant $a$ comes from the ambiguity of the multiplicative factor in $\lambda(1)/\lambda(0)$. Using $\lambda(0) = e^K + e^{-K} = e^{\tilde{K}+a}$, we can fix this constant such that in the very end the partition function reads

$$Z(K) = \left(\frac{1}{2}\right)^N \tilde{Z}(\tilde{K}) = \left(\frac{1}{2}\right)^N \left(\frac{2\cosh(K)}{e^{\tilde{K}}}\right)^{2N} Z(\tilde{K}). \tag{2.32}$$

From this dual relation we can see that if $K \to 0$, we have $\tilde{K} \to \infty$, which means that a disordered phase in the original model (at high temperature) is mapped to an ordered phase in the dual model (and vice versa). The duality relation in Equation (2.30) allows us to analytically determine the critical coupling $K_c$, where the second order phase transition for the Ising model takes place. The transition takes place when $K = \tilde{K} = K_c$, so we can solve Equation (2.30) for $K_c$ and obtain

$$K_c = \frac{\ln(1+\sqrt{2})}{2}. \tag{2.33}$$

The geometrical interpretation of a dual transformation uses the idea of a dual lattice, where the dual model lives. The dual lattice of an arbitrary lattice is constructed by putting a lattice point (designated by a cross) in the interior of every elementary polygon of the original lattice and connecting them by a new dual interaction bond (dashed lines). In Figure 2.3 and 2.4 we see that the

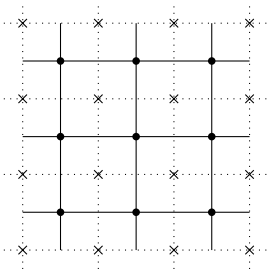

**Figure 2.3:** Dual lattice of square lattice.

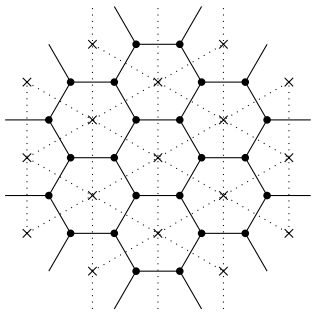

**Figure 2.4:** Dual lattice of the honeycomb lattice.

square lattice is self-dual (in the sense that its dual is also a square lattice) and the dual lattice of the honeycomb lattice is a triangular lattice. Since the duality relation is reciprocal, the dual of the triangular lattice is again a honeycomb lattice. If we want to obtain a duality relation for a spin model on a honeycomb lattice, we need to consider an additional transformation, which is known as the star-triangle-transformation (see Chapter 4).

### 2.3.2 Dualization of the XY Model

We showed that the $q$-state planar clock model on the square lattice is self-dual. Here we want to show that an XY model is mapped to a two-dimensional height model by a duality transformation. Consider an XY model on a square lattice with partition function

$$Z_{\mathrm{XY}}(K) = \left(\int \mathcal{D}\varphi\right) \prod_{\langle x,y\rangle} u(\varphi_y - \varphi_x) = \left(\int \mathcal{D}\varphi\right) \prod_{\langle x,y\rangle} e^{K\cos(\varphi_y - \varphi_x)}, \tag{2.34}$$

where we introduced once again the dimensionless coupling parameter $K = \beta J$ and implicitly gave a definition for the Boltzmann weight $u(\varphi_y - \varphi_x)$. In order to perform the dual transformation we use the Fourier expansion such that

$$u(\varphi_y - \varphi_x) = \sum_{k_{xy}\in\mathbb{Z}} e^{ik_{xy}(\varphi_y - \varphi_x)} \lambda(k_{xy}). \tag{2.35}$$

Applying the same procedure as in Subsection 2.3.1 yields that

$$Z_{\mathrm{XY}}(K) \propto \tilde{Z}_{\mathrm{H.M.}}(\tilde{K}), \tag{2.36}$$

where $\tilde{Z}_{\mathrm{H.M}}(\tilde{K})$ is given by

$$\tilde{Z}_{\mathrm{H.M.}}(\tilde{K}) = \sum_{[\mathrm{h}]} \prod_{\langle \tilde{x},\tilde{y}\rangle} \lambda(|h_{\tilde{x}} - h_{\tilde{y}}|). \tag{2.37}$$

In the previous expression [h] denotes an integer-valued height configuration on the dual lattice, and $\lambda(|h_{\tilde{x}} - h_{\tilde{y}}|)$ is the modified Bessel function given by

$$\begin{aligned}\lambda(|h_{\tilde{x}} - h_{\tilde{y}}|) &= \frac{1}{2\pi}\int_0^{2\pi} e^{K\cos(\varphi)} e^{-i|h_{\tilde{x}} - h_{\tilde{y}}|\varphi}\,\mathrm{d}\varphi \\ &= \frac{1}{2\pi}\int_0^{2\pi} e^{K\cos(\varphi)} \cos(|h_{\tilde{x}} - h_{\tilde{y}}|\varphi)\mathrm{d}\varphi.\end{aligned} \tag{2.38}$$

From the dualization procedure we can see that we turn the angular-valued XY model into a height model, where the degrees of freedom are integer-valued height variables. This transformation does not yield an algebraic relation between the coupling parameter $K$ and the dual coupling parameter $\tilde{K}$, like we had for the $q = 2$ clock model. In order to obtain such a relation we modify the original XY model by applying a Villain-style replacement [7–9],

$$u(\varphi) = e^{K\cos(\varphi)} \mapsto w(\varphi) = \sum_{p\in\mathbb{Z}} e^{-\frac{K}{2}(\varphi - 2\pi p)^2}, \tag{2.39}$$

where $w(\varphi)$ is a $2\pi$-periodic function that is peaked at $\varphi = 0$, like the original XY Boltzmann weight $u(\varphi)$. Thus the physics is qualitatively the same. By using the Poisson summation formula (see appendix A.3), we obtain

$$w(\varphi) = \sum_{p\in\mathbb{Z}} e^{-\frac{K}{2}(\varphi - 2\pi p)^2} = \frac{1}{\sqrt{2\pi K}} \sum_{n\in\mathbb{Z}} e^{in\varphi - \frac{1}{2K}n^2}. \tag{2.40}$$

The partition function can then be written as

$$\begin{aligned}Z_{\mathrm{XY}}(K) &= \left(\int \mathcal{D}\varphi\right) \prod_{\langle x,y\rangle} w(\varphi_y - \varphi_x) \\ &\propto \left(\int \mathcal{D}\varphi\right) \prod_{\langle x,y\rangle} \sum_{n_{xy}\in\mathbb{Z}} e^{in_{xy}(\varphi_y - \varphi_x) - \frac{1}{2K}n_{xy}^2}.\end{aligned} \tag{2.41}$$

Evaluating the integrals over the angles $\varphi_x$ yields the vanishing of the lattice divergence, we have already encountered in Subsection 2.3.1, such that

$$\tilde{Z}_{\mathrm{H.M.}}(\tilde{K}) \propto \sum_{[n_{xy}]}^{*} \prod_{\langle x,y\rangle} e^{-\frac{\tilde{K}}{2}n_{xy}^2}. \tag{2.42}$$

Once again $\sum^*_{[n_{xy}]}$ denotes a summation over all bond configurations which satisfy the constraint and we defined the dual coupling parameter $\tilde{K} = 1/K$. The vanishing lattice divergence enables us to write $n_{xy}$ in terms of integer-valued height variables $[h]$ living on the dual lattice, such that $n_{xy} = h_{\tilde{y}} - h_{\tilde{x}}$. The vanishing lattice divergence guarantees that the integer heights are defined consistently up to an unimportant overall shift. The constrained partition function can then be written as an unconstrained sum over all integer-valued heights

$$\tilde{Z}_{\mathrm{H.M.}}(\tilde{K}) \propto \sum_{[h]} \prod_{\langle \tilde{x},\tilde{y}\rangle} e^{-\frac{\tilde{K}}{2}(h_{\tilde{x}} - h_{\tilde{y}})^2}. \tag{2.43}$$

The duality relation among the coupling variables

$$\tilde{K}K = 1, \tag{2.44}$$

shows that the strong coupling phase of the XY model (large value of $K$) belongs to a weak coupling phase of the height model (small value of $\tilde{K}$).

## 2.4 $F$ Model on a Triangular Lattice ($F_\Delta$ Model)

The $\tilde{F}_\Delta$ model we are going to investigate is equivalent to the so-called $F$ model on a triangular lattice [10], which is a constrained 20-vertex model. Here we give a quick introduction for the $F_\Delta$ model, the equivalence is shown in Section 5.2. Suppose that arrows are placed on bonds of a triangular lattice, such that there are three arrows entering and three arrows leaving each vertex. There exist 20 different configurations of arrows at each vertex. If we identify configurations with all arrows reversed we obtain the 10 distinct configurations shown in Figure 2.5.

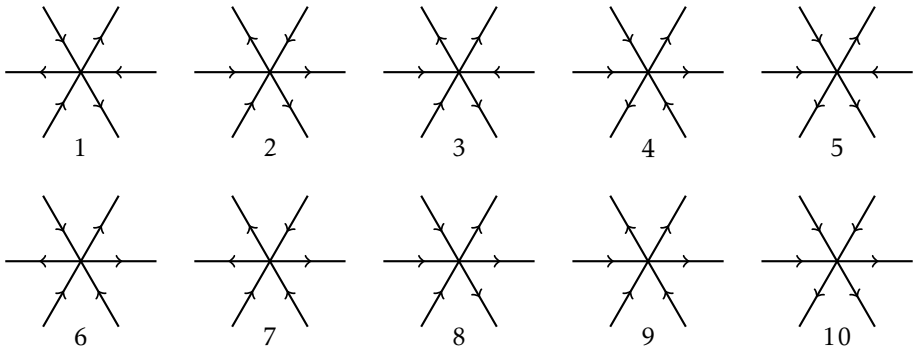


**Figure 2.5:** Ten distinct reversal-symmetric vertex configurations

This is the original 20-vertex model, where we could assign different weights to each of these vertices. The $F_\Delta$ model identifies configurations which are related to each other by rotation and reflection and gives them the same weight. The different vertices are classified as follows

1. 2 vertices, in which ingoing and outgoing arrows are adjacent (vertex 1).

2. 12 vertices, where two incoming arrows are adjacent and the third arrow enters in the opposite way (vertex 2,3,4,5,6,7).

3. 6 vertices, in which the three incoming arrows are adjacent (vertex 8,9,10).

Now we assign energies $\epsilon_0, \epsilon_1, \epsilon_2$ to each of these types of vertices. The first type has energy $\epsilon_0$, which is the ground state energy, the second type has energy $\epsilon_1$, the third one energy $\epsilon_2$, such that $\epsilon_0 < \epsilon_1 < \epsilon_2$. The corresponding Boltzmann weights are given by $w_i = \exp(-\beta\epsilon_i)$. The $F_\Delta$ model was solved analytically by Baxter [10], under the subsidiary condition that the Boltzmann weights satisfy

$$(w_2 - w_1)^2 = w_2(w_0 - w_1). \tag{2.45}$$

## 2.5 Observables

In order to study a statistical model, we are interested in various observables, which provide us with information about macroscopic properties of the system. Interesting observables for the Ising ferromagnetic are, for instance, the thermal expectation value of the energy $\langle \mathcal{H} \rangle$ and the magnetization $\langle \mathcal{M} \rangle$. The internal energy and the magnetization for a specific configuration $[s]$ are defined

as

$$\mathcal{H}_{\text{Ising}}[s] = -J \sum_{\langle x,y \rangle} s_x s_y \tag{2.46}$$

and

$$\mathcal{M}[s] = \sum_x s_x. \tag{2.47}$$

The internal energy $\langle \mathcal{H} \rangle$ is then given by

$$\langle \mathcal{H} \rangle = \sum_{[s]} \mathcal{H}[s] p[s] = \frac{1}{Z(\beta)} \sum_{[s]} \mathcal{H}[s] e^{-\beta \mathcal{H}[s]}. \tag{2.48}$$

Using the specific heat

$$C_V = \left. \frac{\partial \langle \mathcal{H}(T) \rangle}{\partial T} \right|_V \tag{2.49}$$

and the relation

$$-\left. \frac{\partial \langle \mathcal{H}(\beta) \rangle}{\partial \beta} \right|_V = \langle \mathcal{H}^2 \rangle - \langle \mathcal{H} \rangle^2, \tag{2.50}$$

one can derive a fluctuation relation for the energy of the macroscopic system

$$C_V k_B T^2 = \langle \mathcal{H}^2 \rangle - \langle \mathcal{H} \rangle^2 = \langle (\Delta \mathcal{H})^2 \rangle. \tag{2.51}$$

Similar fluctuation relations also hold for other quantities, e.g., for the isothermal susceptibility

$$\chi = \left. \frac{\partial \langle M \rangle}{\partial \mathcal{H}} \right|_T, \tag{2.52}$$

such that one obtains

$$k_B T \chi = \langle \mathcal{M}^2 \rangle - \langle \mathcal{M} \rangle^2. \tag{2.53}$$

For height models there are other interesting quantities namely the winding numbers $W_x$ and $W_y$, which characterize the boundary conditions. The free energy of a system describes quantitatively the capacity of a system to perform work and can be determined from the partition function

$$F(\beta) = -k_B T \log(Z(\beta)). \tag{2.54}$$

Thermodynamic quantities can be calculated by appropriate differentiation of the free energy e.g.

$$\langle \mathcal{H} \rangle = -T^2 \frac{\partial(\frac{F(\beta))}{T})}{\partial T}, \qquad \langle \mathcal{M} \rangle = -\frac{\partial F(\beta)}{\partial H}. \tag{2.55}$$

## 2.6 Phase Transitions

The term phase transition is most commonly used in order to describe transitions between solid, gaseous, and liquid states of matter. A thermodynamical system in a phase has uniform physical properties, which change continuously as a function of some external parameters, such as temperature, pressure or even both. In this chapter we assume this parameter to be the temperature $T$. At a certain critical temperature $T_c$ the statistical system undergoes a phase transition, where certain properties change, often discontinuously. A first order phase transition is characterized by the fact that the first derivative of the free energy with respect to $T$ is discontinuous at the transition temperature. For a second order phase transition the first derivative is continuous, but the second derivative at the critical temperature $T_c$ is characterized by a singularity. Since phase transitions and phase diagrams are difficult to compute analytically, we need simulations in order to describe them quantitatively. The discussion on phase transitions in this subsection is limited to classical statistical mechanics.

### 2.6.1 Disordered Phase and Ordered Phase

The Ising ferromagnet has a second order phase transition, which can be characterized using the magnetization $\langle \mathcal{M} \rangle$ as an order parameter. In the disordered phase ($T > T_c$), adjacent spins of a configuration $[s]$ tend to align themselves independently of each other, such that the overall magnetization of a spin configuration is close to zero ($\mathcal{M}[s] \approx 0$). Below the phase transition ($T < T_c$) multiple different ordered states may appear since they are energetically favorable and adjacent spins tend to align in the same direction. The critical temperature can be estimated by considering the behavior of the order parameter $\mathcal{M}$ as a function of $T$. Using the theoretical picture $\mathcal{M}(T)$ (see Figure 2.6) we can distinguish the ordered phase ($T < T_c$) from the disordered phase ($T > T_c$).

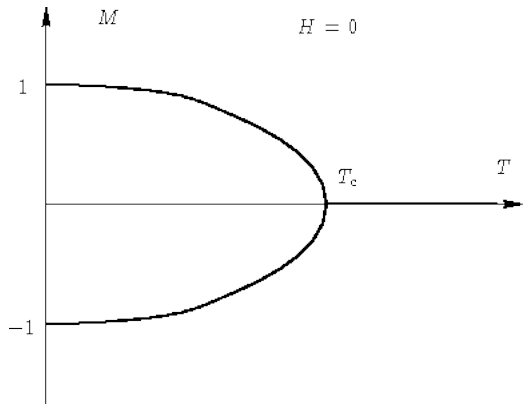


**Figure 2.6:** Magnetization $\mathcal{M}$ per spin as a function of $T$ (Ising model).

Note that for a system with short-range interactions and dimension $d \leq 2$, the Mermin-Wagner theorem states that continuous symmetries cannot be spontaneously broken at finite temperature [11, 12]. Since $U(1)$ models have a continuous $U(1)$ symmetry, the theorem implies that we can not have a completely ordered phase because long-range fluctuations can be created with a small amount of energy. Therefore the simple picture which works for the Ising model needs to be modified for a two-dimensional $U(1)$ model (see Subsection 2.6.5).

### 2.6.2 Spatial Correlations

Even if a system is not ordered, in general there exist regions in which the characteristics of the material are correlated. Since we are interested in spin models, we want to measure regions where spins are spatially correlated. The spatial correlation for an Ising ferromagnet can be measured through a 2-point function

$$\Gamma(r) = \langle s_0 s_r \rangle - \langle s_0 \rangle \langle s_r \rangle, \tag{2.56}$$

where $r$ is the distance between the spin variables. In the limit where $r$ goes to infinity the 2-point correlation function has the form

$$\Gamma(r) \propto \frac{1}{r^\eta} e^{-\frac{r}{\xi}}, \tag{2.57}$$

where $\eta$ is a critical exponent and $\xi = \xi(T)$ is the so-called correlation length, which is a measure for the size of a region in which the Ising spins are correlated. In the disordered phase the correlation length is typically just a few lattice spacings but at the critical temperature $T_c$, the correlation length diverges with a critical exponent $\nu$ such that

$$\lim_{T \to T_c} \xi \propto |T - T_c|^{-\nu}. \tag{2.58}$$

In the ordered phase the correlation length is infinite and the correlation function approaches a constant value.

### 2.6.3 Critical Exponents

Thermodynamical properties of a statistical system can be described by a set of simple power laws in the vicinity of the critical point $T = T_c$.
The Ising ferromagnet has the order parameter $\langle \mathcal{M} \rangle$, the specific heat $C_V$, the susceptibility $\chi$, but also the spatial correlation function $\Gamma$, which have a power law behavior near the critical point. In the vicinity of the critical point these are given by

$$\begin{aligned} \langle \mathcal{M} \rangle &\propto |T - T_c|^{\beta}, T \leq T_c, & \chi &\propto |T - T_c|^{-\gamma}, \\ C_V &\propto |T - T_c|^{-\alpha}, & \xi &\propto |T - T_c|^{-\nu}, \\ \Gamma(r) &\propto \frac{1}{r^{\eta}}, r \to \infty. \end{aligned} \tag{2.59}$$

To summarize, we have introduced five critical exponents $\alpha, \beta, \gamma, \nu$, and $\eta$. In the specific case of the two-dimensional Ising ferromagnetic these take the values

$$\alpha = 0, \qquad \beta = \frac{1}{8}, \qquad \gamma = \frac{7}{4}, \qquad \nu = 1, \qquad \eta = \frac{1}{4}. \tag{2.60}$$

Critical exponents are known analytically only for a certain number of statistical systems, but they are very helpful in order to classify statistical systems into universality classes, where all models of the same class share the same critical behavior.

### 2.6.4 Finite-Size Scaling

When performing numerical simulations on a lattice, the critical behavior of a system can be extracted from the size-dependence of the free energy and other observables near the critical point. According to the finite-size scaling theory (see Fisher [13], Privman [14], or Binder [15]) a scaling ansatz can be written as

$$F(L, T) = L^{-\frac{2-\alpha}{\nu}} \mathcal{F}(\epsilon L^{\frac{1}{\nu}}), \tag{2.61}$$

where $\mathcal{F}$ is some scaling function, $L$ describes the lattice size and $\epsilon = |T - T_c|$. It is important to notice that the critical exponents are defined in infinite lattice volumes. The choice of the scaling variable $z = \epsilon L^{\frac{1}{\nu}}$ is motivated by the fact that the correlation length $\xi \propto \epsilon^{-\nu}$, for $T \to T_c$, is limited by the lattice size $L$, which implies that $\frac{L}{\xi} \propto \epsilon^{\nu} L$, is finite and we might as well take $z = \epsilon L^{\frac{1}{\nu}}$. Appropriate differentiation on the free energy yield the following scaling forms

$$\begin{aligned} \mathcal{M} &= L^{-\frac{\beta}{\nu}} \mathcal{M}^0(\epsilon L^{\frac{1}{\nu}}), \\ \chi &= L^{\frac{\gamma}{\nu}} \chi^0(\epsilon L^{\frac{1}{\nu}}), \\ C_V &= L^{\frac{\alpha}{\nu}} C_V^0(\epsilon L^{\frac{1}{\nu}}). \end{aligned} \tag{2.62}$$

These relations have been derived with the help of the following scaling relations

$$\begin{aligned} (2 - \eta)\nu &= \gamma, \\ \frac{\nu}{2}(\eta + d - 2) &= \beta, \\ 2 - \nu d &= \alpha, \end{aligned} \tag{2.63}$$

and by using certain substitutions in Equation (2.61). The scaling forms (2.62) and the scaling relations in Equation (2.63) are valid only for sufficiently large $L$ and at temperatures close to $T_c$. Exactly at the transition point we have $z \to 0$, and the scaling functions, $\mathcal{M}^0(0), \chi^0(0)$, and $C_V^0(0)$, reduce to proportionality constants, such that we obtain

$$\begin{aligned} \mathcal{M} &\propto L^{-\frac{\beta}{\nu}}, \\ \chi &\propto L^{\frac{\gamma}{\nu}}, \\ C_V &\propto L^{\frac{\alpha}{\nu}}, \text{ at } T = T_c. \end{aligned} \tag{2.64}$$

Note that the scaling functions in (2.62) are universal, apart from the scale factors for their arguments. Since we described the critical behavior of the statistical system, one also needs to explain how to obtain the critical point in the first place. By examining higher-order moments of the magnetization, Binder described a procedure how to derive the critical point of a statistical system [16]. For an Ising model, the Binder cumulant is defined as

$$U_4 = 1 - \frac{\langle \mathcal{M}^4 \rangle}{3\langle \mathcal{M}^2 \rangle^2}, \tag{2.65}$$

such that in the case where the lattice size goes to infinity $U_4 \to 0$ for $T > T_c$ and $U_4 \to 2/3$ for $T < T_c$. For different lattice sizes, curves of $U_4$ cross as a function of the temperature at the fixed point $T = T_c$ and at a certain value $U^*$. Hence by making plots for different lattice sizes one gets a first estimate for $T_c$, from the location of the crossing point. The crossing points for different lattice sizes are going to vary, but nonetheless there should be a general trend towards a fixed critical point $T_c$. Throughout this thesis instead of the original Binder cumulant given in Equation (2.65) we are going to use

$$U_4 = \frac{\langle \mathcal{M}^4 \rangle}{\langle \mathcal{M}^2 \rangle^2}, \tag{2.66}$$

which satisfies the same purpose.

### 2.6.5 Berezinsky-Kosterlitz-Thouless Phase Transition (BKT-transition)

In 2016 the physics Nobel prize was given to John Kosterlitz and David Thouless based on their works on phase transitions of infinite order. A BKT-transition is therefore characterized by the fact that the free energy is an infinitely differentiable function, which makes the transition itself very smooth. This kind of phase transition was extensively investigated in the classical XY model (see Subsection 2.2.2).
For a system with short-range interactions and dimension $d \leq 2$, the Mermin-Wagner theorem states that continuous symmetries cannot be spontaneously broken at finite temperatures [11, 12]. Since the XY model has a $U(1)$ symmetry, the theorem implies that we can not have a completely ordered phase because long-range fluctuations can be created with little energy. Hence the Ising ferromagnet, which has a discrete $\mathbb{Z}_2$ symmetry is allowed to have an ordered phase for $T < T_c$, whereas the classical XY model for $T < T_c$ has a quasi-ordered superfluid phase instead [7]. We conclude that the XY model has two phases, a superfluid phase for $T < T_c$ and a disordered phase for $T > T_c$. At the critical temperature $T_c$ the BKT-transition takes place. The disordered phase is characterized by a short-range correlation with a finite correlation length $\xi < \infty$ such that

$$\Gamma(r) \propto e^{\frac{-r}{\xi}} \tag{2.67}$$

and

$$\lim_{T \downarrow T_c} \xi(T) \propto \exp\left(\frac{\delta}{(T - T_c)^{1/2}}\right). \tag{2.68}$$

As we can see, the correlation length $\xi$ near the critical temperature is not described by Equation (2.58), as it is the case for a finite order phase transition, but by an essential singularity, where $\delta$ is some universal constant. At the critical point itself we enter the superfluid phase, where the correlation length diverges, and the correlation function now reads

$$\Gamma(r) \propto \frac{1}{r^{\eta_c}} \tag{2.69}$$

with $\eta_c = \frac{1}{4}$. For decreasing $T$ we are in the superfluid phase where the correlation function still has a power law behavior, but with a continuously varying critical exponent $\eta$.
Dualizing the classical XY model (resp. a general two-dimensional $U(1)$ model), where sites are parametrized by a continuous angle $\varphi$, leads to a height model where the sites of the lattice are

parametrized by integer-valued variables (subsection 2.3.2). The disordered phase of the XY model ($T > T_c$) is mapped to a rigid phase on the height model which means that the height field is approximately flat. The quasi-ordered superfluid phase of the XY model ($T < T_c$) however is mapped to a rough phase on the height model, where we can also find a continuously varying critical exponent $\eta$. These statements are summarized in Figure 2.7.

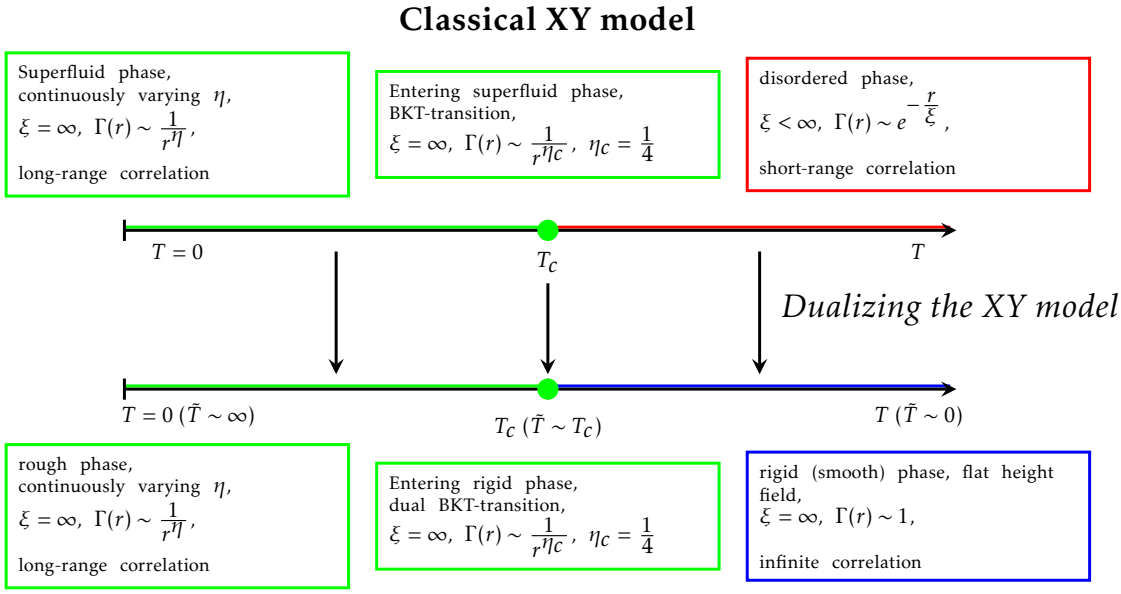


**Figure 2.7:** Classical XY model BKT-transition.

The critical exponents of the BKT-transition were discussed by Kosterlitz in 1974 [17]. Critical exponents refer to infinite volume, but in the classical XY model as $V = L \times L \to \infty$, $\chi$ diverges in the massless phase. The finite-size scaling ansatz for the susceptibility is $\chi \propto L^{\frac{\gamma}{\nu}} = L^{(2-\eta)}$, where the scaling relations were used in the last step. Kosterlitz added a correction term to the finite-size scaling behavior of the susceptibility $\chi$ such that

$$\chi \propto L^{2-\eta_c} (\log(L))^{-2r_e}, \tag{2.70}$$

where $\eta_c = \frac{1}{4}$ and $r_e = \frac{-1}{16}$, in the immediate vicinity of the critical temperature. The additional logarithmic correction term and its critical exponent $r_e$ are very hard to confirm numerically [18]. The best approximation for the additional critical exponent $r_e$ has been obtained by Hasenbusch [19]. He used lattice sizes up to $L = 2048$ and neglected smaller lattices in order to minimize finite-size effects. For $L_{\min} = 512$, and using $r_e$ as a free fit parameter, he obtained $-2r_e = 0.0812(6)$, which is still more than 70 standard deviations smaller than the value predicted by the BKT-theory. The additional logarithmic correction term was the subject of many discussions, since it was hardly possible to confirm it numerically. It was argued by Balog in [20, 21] that the correction term is of the form

$$\ln(\chi) \propto (2-\eta)\ln(L) + \mathcal{O}(Q),$$

where $Q$ is given by $Q = \frac{\frac{\pi^2}{2}}{(\ln(L)+u)^2}$, such that we finally obtain

$$\ln(\chi) \sim (2-\eta)\ln(L) + a\frac{\frac{\pi^2}{2}}{(\ln(L)+u)^2} + b, \tag{2.71}$$

where $\eta, a, b, u$ are fit parameters. The parameter $u$ is a non-universal constant which is measured by taking into account correction terms to the correlation length near the critical point $T_c$

$$\ln(\xi(T)) \sim \frac{\delta}{\sqrt{T - T_c}} - u + c\sqrt{T - T_c}. \tag{2.72}$$

Another indication for a BKT-transition is the behavior of the helicity modulus (or spin stiffness) . The helicity modulus describes the reaction of the system under a twist at the spatial boundary [22]. In order to define the helicity modulus consider a two-dimensional lattice of size $L \times L$, where twisted boundary conditions in one direction are introduced. Consider a bond which crosses the edge of the lattice in the direction where we introduced twisted boundary conditions. Then for the pair of nearest-neighbor sites with $i = L$ and $j = i + 1 = 1$, the weight $w(\varphi_y - \varphi_x)$ is replaced by $w(\varphi_y - \varphi_x + \alpha)$, where $\alpha$ is the twist angle at the boundary. The free energy is minimal at $\alpha = 0$ (no twist). The helicity modulus in its dimensionless form is then defined by the second order derivative of the free energy with respect to $\alpha$ at $\alpha = 0$

$$\Upsilon = \frac{1}{T} \frac{\partial^2}{\partial \alpha^2} F(\alpha)\Big|_{\alpha=0}. \tag{2.73}$$

In the large-volume limit we expect $\Upsilon$ to perform a universal jump at $T_c$. The height of this jump was predicted to be $\frac{2}{\pi}$ [23].

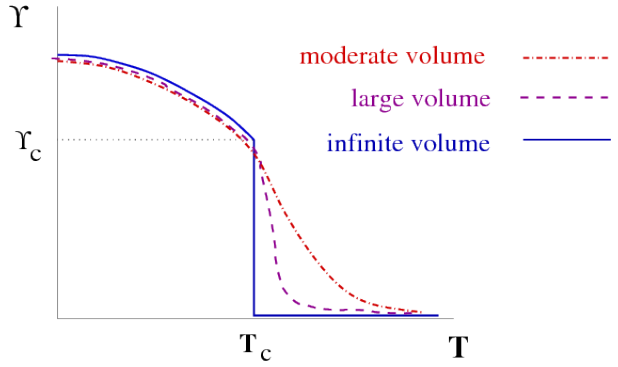


**Figure 2.8:** Helicity modulus $\Upsilon$ as a function of temperature [23].

The region $T \in (0, T_c)$ describes the quasi-ordered superfluid phase with an infinite correlation length, the region $(T_c, \infty)$ characterizes the disordered phase, with a finite correlation length behaving as in Equation (2.67).

# 3 Monte Carlo Simulations

Evaluating the partition function exactly for a large system of interacting spins is a hopeless task. For instance, by just considering 100 interacting Ising spins the partition function contains $2^{100}$ terms. The idea of Monte Carlo sampling is to compute physical quantities we are interested in (observables), by generating spin configurations numerically, such that those spin configurations which have the largest contribution to the partition function are predominantly generated. For a more detailed discussion consider [2, 24].

## 3.1 Markov Chains

The concept of Markov chains is of central importance in Monte Carlo simulations. A Markov chain is a sequence of configurations which begins with an initial configuration $[s^{(1)}]$ and then evolves from $[s^{(i)}]$ to $[s^{(i+1)}]$ recursively by applying some algorithm

$$[s^{(1)}] \to \cdots \to [s^{(N)}]. \tag{3.1}$$

At the end, when computing observables the choice of the initial configuration should not matter. After a certain number of Monte Carlo steps (i.e. iterations from $[s^{(i)}]$ to $[s^{(i+1)}]$), the system has reached equilibrium; from this point on we start measuring an observable $\mathcal{O}$. The measurement of an observable is carried out by averaging over all measurements after approaching equilibrium. Assuming that equilibrium is reached after $M$ iterations $\langle\mathcal{O}\rangle$ is estimated as

$$\overline{\mathcal{O}} = \frac{1}{N-M}\sum_{i=M+1}^{N}\mathcal{O}[s^{(i)}]. \tag{3.2}$$

## 3.2 Measurements and Error Estimations

As in experimental physics, when measuring quantities we have to take into account statistical errors. Let the quantity $\mathcal{O}$ be distributed to a Gaussian with mean value $\langle\mathcal{O}\rangle$ and width $\sigma = \sqrt{\mathrm{Var}(\mathcal{O})}$. Additionally, let us assume that we have $N$ statistically independent observations within equilibrium $\{\mathcal{O}[s^{(i)}]\}_{i=1}^{N}$ of a certain observable $\mathcal{O}$. An unbiased estimator for the mean value is our known expression for a measurement

$$\overline{\mathcal{O}} = \frac{1}{N}\sum_{i=1}^{N}\mathcal{O}[s^{(i)}], \tag{3.3}$$

such that $\langle\overline{\mathcal{O}}\rangle = \langle\mathcal{O}\rangle$. By using the definition of the variance and the assumption that the measurements are independent of each other, the standard deviation of the measurement is given by

$$\Delta\mathcal{O} = \frac{\sigma}{\sqrt{N}}. \tag{3.4}$$

An unbiased estimator of the variance $\sigma^2$ is given by the sample variance $S^2$

$$S^2 = \frac{1}{N-1}\sum_{i=1}^{N}(\mathcal{O}[s^{(i)}] - \overline{\mathcal{O}})^2. \tag{3.5}$$

Consequently $\Delta\mathcal{O}$ can be written as

$$\Delta\mathcal{O} = \frac{S}{\sqrt{N}} = \frac{1}{\sqrt{N(N-1)}}\sqrt{\sum_{i=1}^{N}(\mathcal{O}[\mathrm{s}^{(i)}]-\overline{\mathcal{O}})^2} = \frac{1}{\sqrt{N-1}}\sqrt{\overline{\mathcal{O}^2}-\overline{\mathcal{O}}^2}. \tag{3.6}$$

The ideal Monte Carlo algorithm would create a Markov chain of statistically independent configurations, but since a new configuration is generated from the previous one, subsequent configurations are correlated. This means that the true statistical error is larger than the naive estimate of the standard deviation. In order to take into account correlations of subsequently generated observations we modify the standard deviation by

$$\Delta\mathcal{O}^2 = \frac{s^2}{N}(1+\frac{2\tau_{\mathcal{O}}}{\delta t}) = \Delta\mathcal{O}^2_{\text{naive}}(1+\frac{2\tau_{\mathcal{O}}}{\delta t}), \tag{3.7}$$

where we introduced the integrated autocorrelation time $\tau_{\mathcal{O}}$ which is measured in units of $\delta t$. The additional term in $\Delta\mathcal{O}^2$ can be considered as a correction term for the true statistical error.

## 3.3 Autocorrelation

A normalized autocorrelation function is used in order to estimate the number $\tau$ of iterations that separate statistically independent configurations. Consider the Markov chain as a statistical system evolving in time. The normalized autocorrelation function for some observable $\mathcal{O}$ (within equilibrium) is defined as

$$\phi(t) = \frac{\langle\mathcal{O}[\mathrm{s}^{(t_0)}]\mathcal{O}[\mathrm{s}^{(t_0+t)}]\rangle - \langle\mathcal{O}\rangle^2}{\langle\mathcal{O}^2\rangle - \langle\mathcal{O}\rangle^2},$$

with the properties that $\phi(0) = 1$, $\lim_{t\to\infty}\phi(t) = 0$ and $\phi(t)$ decays monotonically with increasing time $t$. The long-time behavior of the normalized relaxation function is exponential such that

$$\phi(t) \propto e^{-\frac{t}{\tau}}, \qquad t \to \infty. \tag{3.8}$$

As one approaches a second order phase transition the autocorrelation time $\tau$ increases. This dynamical critical behavior, also called critical slowing down, can be expressed in terms of a power law,

$$\tau \propto \xi^z \propto |T - T_c|^{-\nu z}, \tag{3.9}$$

where $z$ is the so-called dynamical critical exponent characterizing the efficiency of a Monte Carlo algorithm.
For the error analysis (see Equation (3.7)), the relevant quantity is the integrated autocorrelation time $\tau_{\mathcal{O}}$

$$\frac{\tau_{\mathcal{O}}}{\delta t} = \sum_{k=1}^{\infty}\phi(t). \tag{3.10}$$

Note that $\tau_{\mathcal{O}} = \tau$ if the autocorrelation function is purely exponential $\phi(t) = e^{-t/\tau}$. Since $\phi(t)$ becomes noisy for $t \gg \tau_{\mathcal{O}}$, the sum in Equation (3.10) can behave badly when $t$ is large. Thus the sum should be truncated self-consistently, as the summation proceeds.

## 3.4 Detailed Balance and Ergodicity

In order to ensure that a Monte Carlo algorithm converges to the correct equilibrium distribution, it is sufficient that the algorithm obeys ergodicity and detailed balance. Ergodicity means that all possible configurations which contribute to the partition function should theoretically be accessible.

This condition is necessary since we must be able to take into account all possible contributions. Detailed balance means that

$$p[\mathrm{s}]w[\mathrm{s},\mathrm{s}'] = p[\mathrm{s}']w[\mathrm{s}',\mathrm{s}], \tag{3.11}$$

where $p[\mathrm{s}]$ is the probability for the system to be in configuration [s], defined in Equation (2.3), and $w[\mathrm{s},\mathrm{s}']$ is the transition probability to turn the configuration [s] into [s′]. The transition probability is normalized to

$$\sum_{[\mathrm{s}']} w[\mathrm{s},\mathrm{s}'] = 1, \tag{3.12}$$

since the algorithm necessarily turns a configuration [s] into some other configuration [s′]. In order to ensure that the algorithm converges towards the equilibrium distribution $p[\mathrm{s}]$, we require that the distribution $p[\mathrm{s}]$ is an eigenvector of the transition matrix $w[\mathrm{s},\mathrm{s}']$ with eigenvalue 1

$$\sum_{[\mathrm{s}]} p[\mathrm{s}]w[\mathrm{s},\mathrm{s}'] = p[\mathrm{s}']. \tag{3.13}$$

Using the detailed balance condition (3.11), and the normalization of the transition probability we see that this requirement is fulfilled

$$\sum_{[\mathrm{s}]} p[\mathrm{s}]w[\mathrm{s},\mathrm{s}'] = \sum_{[\mathrm{s}]} p[\mathrm{s}']w[\mathrm{s}',\mathrm{s}] = p[\mathrm{s}']. \tag{3.14}$$

By using ergodicity one can show that such an eigenvector exists, is unique, and that the equilibrium distribution is therefore indeed approached asymptotically.

## 3.5 Algorithms

### 3.5.1 Single Spin Flip Method (Metropolis Algorithm)

The Metropolis algorithm is a simple algorithm, where a new configuration [s′] is randomly chosen based on the old configuration [s], depending on the energy differences. If the new configuration is energetically favorable, it is accepted which means that

$$\Delta\mathcal{H} = \mathcal{H}[\mathrm{s}'] - \mathcal{H}[\mathrm{s}] < 0 \qquad \Longrightarrow\ w[\mathrm{s},\mathrm{s}'] = 1. \tag{3.15}$$

If the new energy is larger, we accept the new configuration with a certain probability

$$\Delta\mathcal{H} = \mathcal{H}[\mathrm{s}'] - \mathcal{H}[\mathrm{s}] > 0 \qquad \Longrightarrow\ w[\mathrm{s},\mathrm{s}'] = e^{-\beta\Delta\mathcal{H}}. \tag{3.16}$$

The algorithm is ergodic since every spin configuration is accessible with a certain non-vanishing probability. In order to show detailed balance consider the case where $\mathcal{H}[\mathrm{s}] - \mathcal{H}[\mathrm{s}'] > 0$, such that $\mathcal{H}[\mathrm{s}'] - \mathcal{H}[\mathrm{s}] < 0$ and $w[\mathrm{s},\mathrm{s}'] = 1$. Then detailed balance is fulfilled since

$$p[\mathrm{s}']w[\mathrm{s}',\mathrm{s}] = \frac{e^{-\beta\mathcal{H}[\mathrm{s}']}}{Z(\beta)} e^{-\beta(\mathcal{H}[\mathrm{s}]-\mathcal{H}[\mathrm{s}'])} = p[\mathrm{s}]\cdot 1 = p[\mathrm{s}]w[\mathrm{s},\mathrm{s}']. \tag{3.17}$$

In the simple case of the Ising ferromagnet one visits every spin one by one and proposes to flip it. The change of energy can be directly calculated by considering neighboring spins. After visiting every spin we have completed one Metropolis sweep. The Metropolis algorithm has a dynamical critical exponent (see Equation (3.9)) of $z \approx 2$, which leads to a bad critical slowing down behavior. Efficient cluster algorithms, on the other hand, can reach $z \approx 0$.

### 3.5.2 Cluster Flip Method (Swendsen-Wang Cluster Algorithm)

Cluster flipping methods describe an entire class of algorithms which attempt to create statistically independent configurations, by flipping clusters of spins in an intelligent way, instead of simply attempting single spin flips. For instance, when considering the Ising model, one can apply the so-called Swendsen-Wang cluster algorithm, where a link between spins is frozen or not depending on the orientation of the adjacent spins. In general we may begin with an initial spin configuration. Then we proceed through the lattice, freezing links between each pair of spins with a certain probability $p$. One identifies all clusters which are produced by a connected network of links, these are then flipped with a probability of 0.5. Next the bonds are erased and a new spin configuration has been produced, which completes one sweep of the algorithm.
Let us work out the cluster building prescription for the Ising model. In the Ising model, no links are frozen between anti-parallel spins, therefore all spins in a cluster point in the same direction. In the case of parallel spins the contribution to the partition function is given by $e^{\beta J}$. This particular contribution is now split up into a piece where the link between the two spins is frozen and a piece where the link is not frozen (see Figure 3.1).

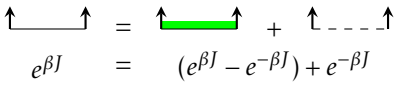


**Figure 3.1:** Bond Splitting.

Hence the probability for a link to be frozen between two parallel spins is given by

$$p = 1 - e^{-2\beta J}. \tag{3.18}$$

Using this prescription we construct clusters in which all spins are pointing in the same direction. In order to show ergodicity, consider an arbitrary configuration [s′]. This configuration [s′] is directly reachable (in one step) from any other configuration [s] if no links are frozen (which can happen with a small but non-vanishing probability) and flip every spin in [s] which is anti-parallel compared to [s′].
If we want to show detailed balance, the algorithm needs to fulfill Equation (3.11). Since the corresponding terms for the probability and the transition probability factorize, it is sufficient to consider only 2 spins which are next to each other. We need to consider 3 different situations where one pair of spins (parallel or anti-parallel) transforms to another pair of spins (also either parallel or anti-parallel), and for each of these situations we need to show that Equation (3.11) is satisfied. In the following we denote two anti-parallel spins as $\uparrow\downarrow$ and two parallel spins as $\uparrow\uparrow$.

1. $\uparrow\downarrow \leftrightarrow \uparrow\downarrow$

$$p[\uparrow\downarrow]w[\uparrow\downarrow,\uparrow\downarrow] = p[\uparrow\downarrow]w[\uparrow\downarrow,\uparrow\downarrow]$$

2. $\uparrow\uparrow \leftrightarrow \uparrow\uparrow$

$$p[\uparrow\uparrow]w[\uparrow\uparrow,\uparrow\uparrow] = p[\uparrow\uparrow]w[\uparrow\uparrow,\uparrow\uparrow]$$

3. $\uparrow\downarrow \leftrightarrow \uparrow\uparrow$

$$p[\uparrow\downarrow]w[\uparrow\downarrow,\uparrow\uparrow] = p[\uparrow\uparrow]w[\uparrow\uparrow,\uparrow\downarrow]$$
$$\frac{e^{-\beta J}}{Z(\beta)}\frac{1}{2} = \frac{e^{\beta J}}{Z(\beta)}\frac{1}{2}(1-p)$$

As we see, all three situations satisfy the detailed balance condition. Therefore we conclude that the Swendsen-Wang cluster algorithm applied to the Ising model obeys ergodicity and detailed balance.

# 4 The Honeycomb Lattice

At this point we have gathered some basic knowledge about classical statistical mechanics and Monte Carlo algorithms. The $\tilde{F}_\Delta$ model is defined on a honeycomb lattice where we associate an integer-valued spin to each lattice site. Therefore the $\tilde{F}_\Delta$ model belongs to the class of height models. Before going deeper into the formulation of the $\tilde{F}_\Delta$ model, we investigate some basic properties of the honeycomb lattice.

## 4.1 Description and Properties

The honeycomb lattice is an arrangement of hexagons, with spins residing on the lattice sites, which are connected by an interaction bond. The lattice can be defined as

$$\Lambda := \{\vec{x} \in \mathbb{R}^2 : \vec{x} = n_1\vec{e}_1 + n_2\vec{e}_2 \pm \vec{z}, \vec{e}_1 = \begin{pmatrix}0\\1\end{pmatrix}, \vec{e}_2 = \frac{1}{2}\begin{pmatrix}\sqrt{3}\\1\end{pmatrix}, \vec{z} = \frac{1}{6}\begin{pmatrix}\sqrt{3}\\3\end{pmatrix}, n_1, n_2 \in \mathbb{Z}\}. \tag{4.1}$$

A hexagon is a six-sided regular polygon, and can be translated by some vectors $\vec{e}_1, \vec{e}_2$ in order to

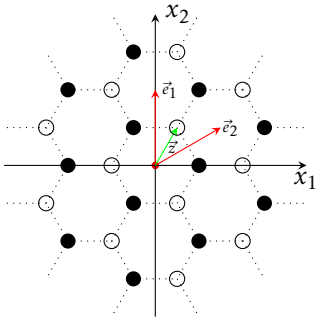


**Figure 4.1:** Honeycomb lattice.

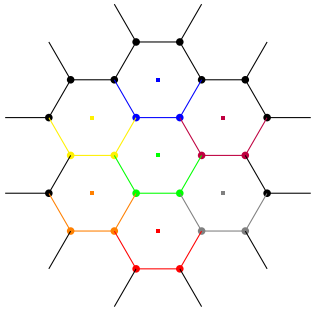

**Figure 4.2:** Bonds, Spins, Hexagons.

generate a honeycomb lattice. As we see from its definition, the lattice $\Lambda$ can be expressed in terms of two disjoint subsets, in other words, the honeycomb lattice is **bipartite** and therefore decomposes into two sublattices

$$\begin{aligned}\Lambda &= A_\bullet \dot{\cup} B_\circ \\ &= \{\vec{x} \in \Lambda : \vec{x} = n_1\vec{e}_1 + n_2\vec{e}_2 - \vec{z}\} \dot{\cup} \{\vec{x} \in \Lambda : \vec{x} = n_1\vec{e}_1 + n_2\vec{e}_2 + \vec{z}\}.\end{aligned}$$

The $A_\bullet$ sublattice is denoted by black dots and the $B_\circ$ sublattice is denoted by white dots (respectively open circles) in Figure 4.1. Assuming a two-dimensional honeycomb lattice of infinite size (i.e. neglecting boundary effects), it is easy to see that we can associate 2 spins and 3 bonds with each hexagon (see Figure 4.2). By definition, the honeycomb lattice is not a Bravais lattice, i.e., it can not be expressed as an integer linear combination of some basis vectors $\vec{a}_1, \vec{a}_2$. Nonetheless, we could construct a two-dimensional Bravais lattice out of the honeycomb lattice, when we bind lattice points together in a specific way (see Figure 4.3). The unit cell, which has the shape of a parallelogram would consist of two lattice points and the translation vectors $\vec{e}_1, \vec{e}_2$ used before can again be used in order to generate the lattice by translating the unit cell along these vectors.

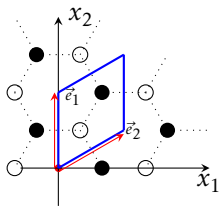


**Figure 4.3:** Unit cell and primitive vectors.

## 4.2 Duality Transformation and Star-Triangle Transformation

In 1944 Onsager introduced the star-triangle transformation for the honeycomb lattice [25], which can also be considered an integrating-out step of one of the two sublattices. In order to perform this transformation, the nearest-neighbor interaction of the spins needs to factorize, which happens to be the case for the $\tilde{F}_\Delta$ model.

### 4.2.1 The Star-Triangle Transformation

The square lattice is self-dual, such that the dual transformation yields a high-temperature-low-temperature relation. Using this transformation for the Ising model on a square lattice one also obtains an analytic result for the critical temperature - dual transforming the honeycomb lattice, would not yield such a relation. Nonetheless, combining the dual transformation with the star-triangle transformation (also abbreviated with $\star$-$\Delta$ transformation), one also obtains a high-temperature-low-temperature relation. Throughout this thesis a dual transformation of a honeycomb lattice is defined to combine the classical dual transformation with a star-triangle transformation.
We have seen that the honeycomb lattice is bipartite, i.e., it decomposes into two sublattices, where the sublattice $A_\bullet$ is represented by black dots and the sublattice $B_\circ$ is represented by white dots (respectively open circles, see Figure 4.1). Since we are dealing with nearest-neighbor interactions, each white site (each point of $B_\circ$) interacts with 3 black sites (3 points of $A_\bullet$) and vice versa. The interaction between a white site and a black site is given by some symmetric function $u$ of the spin differences such that


$$\hat{=} u(|s_y - s_x|),$$

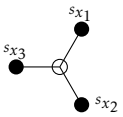


$$\hat{=} u(|s_y - s_{x_1}|)u(|s_y - s_{x_2}|)u(|s_y - s_{x_3}|).$$

Assuming that both sublattices are symmetric, one is tempted to express the partition function $Z(\beta)$ as a function of one sublattice only. Using a general weight $w = w[\mathrm{s}]$ instead of the physically motivated exponential of the Hamiltonian, one can write

$$Z(\beta) = \sum_{[\mathrm{s}]} w[\mathrm{s}] = \sum_{x \in A_\bullet} \sum_{y \in B_\circ} \prod_{\langle x,y \rangle} u(|s_x - s_y|) = \sum_{x \in A_\bullet} \prod_{\langle x_i, x_j \rangle} b(|s_{x_j} - s_{x_i}|). \tag{4.2}$$

What happens algebraically is that we **integrated out** the points of the $B_\circ$ sublattice and expressed the interaction between the $B_\circ$ sublattice and the $A_\bullet$ sublattice as an interaction between spins of the $A_\bullet$ sublattice only. In order to perform this transformation we require a special form of $u = u(|s_y - s_x|)$, such that the sum over the interior points factorizes (see Figure 4.4). Executing this transformation, we see that we geometrically turn a honeycomb lattice into a triangular lattice.

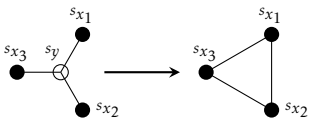


$$\sum_{s_y} u(|s_{x_1} - s_y|)u(|s_{x_2} - s_y|)u(|s_{x_3} - s_y|) = b(|s_{x_1} - s_{x_2}|)b(|s_{x_2} - s_{x_3}|)b(|s_{x_3} - s_{x_1}|)$$

**Figure 4.4:** Star-triangle transformation. We integrate out the spin variable $s_y$.

### 4.2.2 Dual Transformation of the Honeycomb Lattice

Since we have worked out the concepts of the dual transformation and the star-triangle transformation ($\star$-$\Delta$ transformation), we are now able to construct a closed loop of transformations starting with the honeycomb lattice (see Figure 4.5). It is important to mention that the partition functions

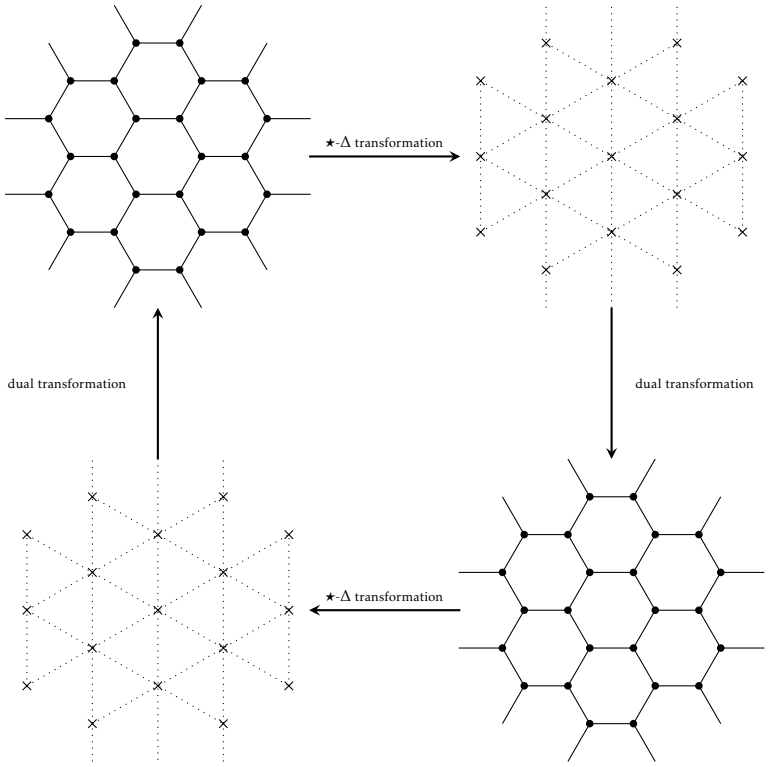


**Figure 4.5:** Dual transformation for the honeycomb lattice.

**do not** look the same at any stage of the transformation. This will be discussed in more detail in Section 5.3. As a side remark we also want to mention that this dualization procedure could be extended even further. By additionally introducing the Kagome lattice, the diced lattice, the decorated lattice, and by introducing the decoration iteration transformation, one can even further extend the loop transformation. The interested reader is referred to [26], for a more detailed discussion of these topics.

## 4.3 Boundary Conditions

Since lattice simulations are performed on finite systems, one important question to answer is how to treat edges or boundaries of the lattice. Boundaries can be effectively eliminated by wrapping the two-dimensional lattice around a torus. In order to impose periodic boundary conditions we identify spins and spin interactions on the boundaries in an unambiguous way. We start by superimposing a hexagon over the honeycomb lattice and cutting off the rest. Now we identify opposite edges (denoted by the same color in Figure 4.6 with labels $W_A$, $W_B$, $W_C$). Assume we have a height model where each lattice site is characterized by an integer-valued height variable. Then the quantities $W_A, W_B, W_C$ characterizing the boundary conditions are integer-valued winding numbers, which describe a shift of the height variables at the boundaries. Copying the hexagons and gluing them next to each other, one also notices that one of the winding numbers is determined by the other two (compare Figure 4.7)

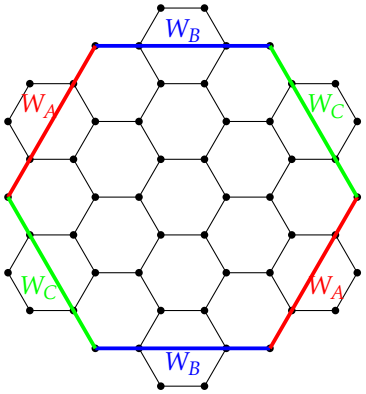


**Figure 4.6:** Boundary condition torus.

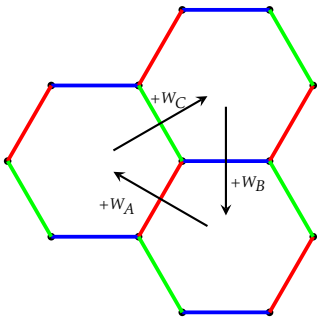


**Figure 4.7:** Relation between the boundary conditions.

$$W_A + W_B + W_C = 0. \tag{4.3}$$

We come to realize that we are actively dealing with only two different boundary conditions. In order to wrap the hexagon around the torus, we cut the existing hexagon into pieces and glue them together in a specific way (see Figure 4.8). Using this construction, we end up with two independent boundary conditions on a parallelogram which are characterized by winding numbers ($W_x$ and $W_y$). The parallelogram is homeomorphic to the torus so we can wrap the parallelogram around it and realize that the edges match each other. Since the torus has interesting properties which are important throughout this thesis we want to mention some of them. Note that configurations of a height model for a system with periodic boundary conditions can be separated into sectors classified by their winding numbers $(W_x, W_y)$. Consider a parallelogram-shaped lattice of size $L \times L$ and describe height variables by some $(x, y)$ coordinates adapted to the constructed parallelogram, such that $h = h_{x,y}$ (see Figure 4.9). If we translate the spin by a lattice size $L$ in either $\hat{\mathbf{x}}$ or $\hat{\mathbf{y}}$ direction, we need to take into account that the height field obeys the boundary conditions $h_{x+L,y} = h_{x,y} + W_y$ and $h_{x,y+L} = h_{x,y} + W_x$. The partition function ends up being a sum over all possible height configurations of all different sectors $(W_x, W_y)$.
We showed that by dualizing an XY model, where we have a twist angle $\alpha$ and a helicity modulus $\Upsilon$, we obtain a height model (see Subsections 2.6.5 and 2.3.2). The helicity modulus can be expressed in terms of the height model as

$$\Upsilon = \langle W_x^2 \rangle, \tag{4.4}$$

where $W_x$ is the integer-valued shift at the boundary in one direction [19].

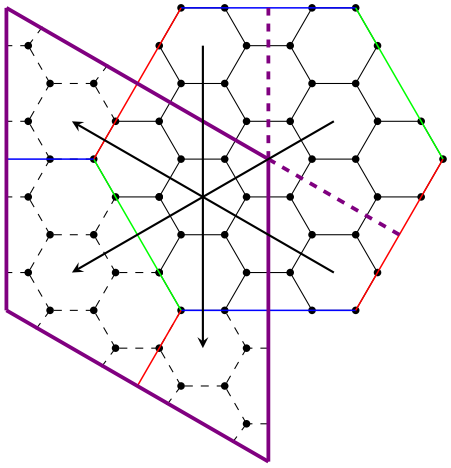

**Figure 4.8:** Create a parallelogram by cutting the hexagon into pieces.

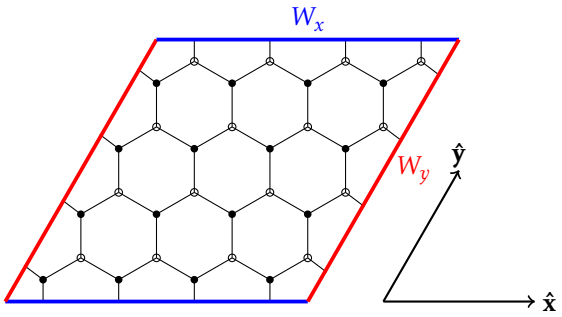


**Figure 4.9:** Parallelogram of size $4 \times 4$, obtained from the initial hexagon.

### 4.3.1 The Torus

The two-dimensional torus is a 2-manifold which can be defined as

$$\mathbb{T}^2 = S^1 \times S^1. \tag{4.5}$$

Its fundamental group is given by

$$\pi_0(\mathbb{T}^2) = \pi_0(S^1 \times S^1) = \pi_0(S^1) \times \pi_0(S^1) = \mathbb{Z} \times \mathbb{Z}. \tag{4.6}$$

The fundamental group describes the classes of homotopy equivalent closed paths on the torus. A closed path on the torus which can be shrunk to a point is called null-homotopic. A loop (respectively a cluster) with non-trivial winding number changes the winding numbers $(W_x, W_y)$ of the statistical system, and takes us to another sector of the statistical system. Whether $W_x$ or $W_y$ is changed depends on the way the cluster wraps around the torus. For example, if it wraps around the torus in the horizontal direction (i.e. it crosses the red line in Figure 4.9) the winding number $W_x$ changes.

# 5 The $\tilde{F}_\Delta$ Model

## 5.1 Definition of the $\tilde{F}_\Delta$ Model

We have set up the honeycomb lattice, where we can now impose the $\tilde{F}_\Delta$ model and specify its properties. The $\tilde{F}_\Delta$ model belongs to the class of height models, i.e., each lattice site hosts an integer-valued height variable. It imposes nearest-neighboring couplings with the interaction term

$$u(h_x - h_y) = \delta_{h_x - h_y, 1} + \delta_{h_x - h_y, -1} = \begin{cases} 1, & \text{if } |h_x - h_y| = 1, \\ 0, & \text{otherwise,} \end{cases} \tag{5.1}$$

such that the partition function on an infinite honeycomb lattice is given by

$$Z = \sum_{[\mathrm{h}]} \prod_{\langle x,y \rangle} u(h_y - h_x) = \Big(\prod_{x \in A_\bullet} \sum_{h_x \in \mathbb{Z}}\Big)\Big(\prod_{y \in B_\circ} \sum_{h_y \in \mathbb{Z}}\Big) \prod_{\langle x,y \rangle} u(h_y - h_x). \tag{5.2}$$

We see that nearest-neighbors are constrained to a height difference of $\pm 1$. Next-to-nearest-neighbors thus have a height difference of $\pm 2$ or 0 and the ones with $\pm 2$ are assigned the smaller Boltzmann weight. The Hamiltonian is given by

$$\beta \mathcal{H}[\mathrm{h}] = \frac{K}{4} \sum_{[i,j]} (h_i - h_j)^2 = \frac{K}{4} \left( \sum_{[x_i, x_j]} (h_{x_i} - h_{x_j})^2 + \sum_{[y_i, y_j]} (h_{y_i} - h_{y_j})^2 \right), \tag{5.3}$$

where $[i, j]$ indicates pairs of next-nearest-neighbors on both sublattices and we absorb the temperature $T$ in the definition of the coupling parameter $K$. Consequently, the partition function takes the form

$$\begin{aligned} Z(K) &= \sum_{[\mathrm{h}]} \left( \prod_{\langle x,y \rangle} u(h_y - h_x) \right) \exp(-\beta \mathcal{H}[\mathrm{h}]) \\ &= \Big(\prod_{x \in A_\bullet} \sum_{h_x \in \mathbb{Z}}\Big)\Big(\prod_{y \in B_\circ} \sum_{h_y \in \mathbb{Z}}\Big) \prod_{[x_i, x_j]} \exp\Big(-\frac{K}{4}(h_{x_i} - h_{x_j})^2\Big) \prod_{[y_i, y_j]} \exp\Big(-\frac{K}{4}(h_{y_i} - h_{y_j})^2\Big) \prod_{\langle x,y \rangle} u(h_y - h_x). \end{aligned} \tag{5.4}$$

The system has a global $\mathbb{Z}$ symmetry: we can translate each height variable by a fixed integer-value $n$. By executing $h_x \mapsto h_x + n$, the partition function would stays the same.

## 5.2 Equivalence of the $\tilde{F}_\Delta$ Model and the $F_\Delta$ Model

Consider the $\tilde{F}_\Delta$ Model with its constraints defined previously. To each of the $\pm 1$ steps between neighboring height variables we assign an arrow from the lower height value to the higher one. This leads to arrow conservation on each hexagon of the honeycomb lattice, meaning that the sum of positive and negative steps around every hexagon evaluates to zero, which is related to the fact that the sum of the height differences for null-homotopic loops yields 0. If we rotate every arrow of a hexagon consistently by an angle of 90 degrees we recognize that we obtain a 20 vertex model on a triangular lattice (see Figure 5.1). Furthermore, we have the same energy distribution as the $F_\Delta$ model (see Section 2.4), but the additional constraint which allows to solve the $F_\Delta$ model analytically is not fulfilled in our case. Therefore we have a one-to-one correspondence between the $F_\Delta$ model and the $\tilde{F}_\Delta$ model.

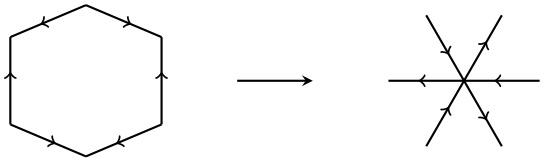

**Figure 5.1:** Transformation of a ground state configuration of the $\tilde{F}_\Delta$ model into the ground state configuration of the $F$ model on a triangular lattice.

## 5.3 Dual Transformation for the Honeycomb Lattice

### 5.3.1 Step 1)

Now we want to execute the dual transformation described in Subsection 4.2.2 on the $\tilde{F}_\Delta$ model, starting from the honeycomb lattice with torus boundary conditions. The dualization procedure is executed for the case $K = 0$, since the interaction between next-nearest-neighbors does not allow for a star-triangle-transformation. For the sake of clarity, we do not implement twisted boundary conditions and therefore we have no twist angle $\alpha$ (see Subsection 2.6.5). The previously presented partition function (5.2) needs to be modified such that it takes into account all sectors characterized by their winding numbers

$$Z = Z(K=0) = \sum_{W_x\in\mathbb{Z}} \sum_{W_y\in\mathbb{Z}} \Big(\prod_{\substack{x\in A_\bullet \\ x\neq\tilde{x}}} \sum_{h_x\in\mathbb{Z}}\Big)\Big(\prod_{x\in B_\circ} \sum_{h_y\in\mathbb{Z}}\Big) \tilde{\prod_{\langle x,y\rangle}} u(h_y - h_x). \tag{5.5}$$

We sum over $W_x$ and $W_y$ in order to take into account all the possible integer-valued winding numbers in both directions. The modified product term $\tilde{\prod}_{\langle x,y\rangle}$ takes into account the contributions of the boundary, so for instance if the interaction bond between two sites crosses the boundary horizontally we have to include an additional summand to the interaction term: $u(h_x - h_y) \mapsto u(h_x - h_y - W_y)$. We exclude one summation over an arbitrary height variable $h_{\tilde{x}}$ and fix it, in order to get rid of the $\mathbb{Z}$-symmetry the overall system has. Otherwise the partition function would be ill-defined.

### 5.3.2 Step 2)

Now we execute the integrate out procedure described in Subsection 4.2, and end up with a height model on a triangular lattice, with partition function

$$Z = \sum_{W_x\in\mathbb{Z}} \sum_{W_y\in\mathbb{Z}} \Big(\prod_{\substack{x\in A_\bullet \\ x\neq\tilde{x}}} \sum_{h_x\in\mathbb{Z}}\Big) \tilde{\prod_{\langle x_i,x_j\rangle}} b(h_{x_j} - h_{x_i}), \tag{5.6}$$

where $b(h_{x_j} - h_{x_i})$ is the interaction term between the points of the $A_\bullet$ sublattice. The interaction term $b$ also takes into account contributions from $W_x$ and $W_y$, if indicated by the product term, and reads

$$\begin{aligned} b(h_{x_j} - h_{x_i}) &= \sqrt[3]{2}\,\delta_{h_{x_j}-h_{x_i},0} + \frac{1}{\sqrt[6]{2}}\big(\delta_{h_{x_j}-h_{x_i},-2} + \delta_{h_{x_j}-h_{x_i},2}\big) \\ &= \begin{cases} \sqrt[3]{2}, & \text{if } |h_{x_j} - h_{x_i}| = 0 \\ \frac{1}{\sqrt[6]{2}}, & \text{if } |h_{x_j} - h_{x_i}| = 2 \\ 0, & \text{otherwise.} \end{cases} \end{aligned} \tag{5.7}$$

### 5.3.3 Step 3)

The dualization procedure described in Subsection 2.3 turns the height model on a triangular lattice into a generalized XY model on the honeycomb lattice. In order to do this we express $b$ as some

Fourier coefficient of a $2\pi$-periodic function $f_{2\pi}$ (see appendix A.1), such that

$$b(h_{x_j} - h_{x_i}) = \frac{1}{2\pi} \int_0^{2\pi} e^{-i(h_{x_j} - h_{x_i})\varphi_{x_i x_j}} f_{2\pi}(\varphi_{x_i x_j}) d\varphi_{x_i x_j}, \tag{5.8}$$

where $\varphi_{x_i x_j}$ can be treated as a bond variable interacting with $h_{x_j}$ and $h_{x_i}$, with an orientation from site $x_i$ to site $x_j$ (thus $\varphi_{x_i x_j} = -\varphi_{x_j x_i}$). In order to do this in a consistent manner we need to define an orientation among the dual variables. We define the orientation in figure 5.2.

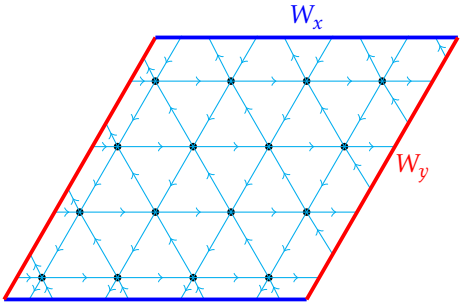


**Figure 5.2:** Triangular lattice on a parallelogram with orientations for the links connecting dual variables.

Keeping in mind the relations of the number of hexagons, height variables, and interaction bonds mentioned in Section 4.1, and using $H$ as the number of hexagons in the honeycomb lattice, one obtains

$$\begin{aligned} Z &= \sum_{W_x \in \mathbb{Z}} \sum_{W_y \in \mathbb{Z}} \Big( \prod_{\substack{x \in A_\bullet \\ x \neq \tilde{x}}} \sum_{h_x \in \mathbb{Z}} \Big) \tilde{\prod_{\langle x_i, x_j \rangle}} b(h_{x_j} - h_{x_i}) \\ &= \sum_{W_x \in \mathbb{Z}} \sum_{W_y \in \mathbb{Z}} \Big( \prod_{\substack{x \in A_\bullet \\ x \neq \tilde{x}}} \sum_{h_x \in \mathbb{Z}} \Big) \tilde{\prod_{\langle x_i, x_j \rangle}} \frac{1}{2\pi} \int_0^{2\pi} e^{-i\varphi_{x_i x_j}(h_{x_j} - h_{x_i})} f_{2\pi}(\varphi_{x_i x_j}) d\varphi_{x_i x_j} \\ &= \Big(\frac{1}{2\pi}\Big)^{3H} \Big( \prod_{\langle x_i, x_j \rangle} \int_0^{2\pi} d\varphi_{x_i x_j} f_{2\pi}(\varphi_{x_i x_j}) \Big) \sum_{W_x \in \mathbb{Z}} \sum_{W_y \in \mathbb{Z}} \Big( \prod_{\substack{x \in A_\bullet \\ x \neq \tilde{x}}} \sum_{h_x \in \mathbb{Z}} \Big) \tilde{\prod_{\langle x_i, x_j \rangle}} e^{-i\varphi_{x_i x_j}(h_{x_j} - h_{x_i})}. \end{aligned} \tag{5.9}$$

At this point we can evaluate the sums over all but one height variable on the $A_\bullet$-lattice and also the sums over the two boundary conditions. Using the formula for the Dirac comb (appendix A.2) we obtain

$$\begin{aligned} Z &= \Big(\frac{1}{2\pi}\Big)^{3H} \Big( \prod_{\langle x_i x_j \rangle} \int_0^{2\pi} d\varphi_{x_i x_j} f_{2\pi}(\varphi_{x_i, x_j}) \Big) \sum_{W_x \in \mathbb{Z}} \sum_{W_y \in \mathbb{Z}} \Big( \prod_{\substack{x \in A_\bullet \\ x \neq \tilde{x}}} \sum_{h_x \in \mathbb{Z}} \Big) \tilde{\prod_{\langle x_i, x_j \rangle}} e^{-i\varphi_{x_i x_j}(h_{x_j} - h_{x_i})} \\ &= \Big(\frac{1}{2\pi}\Big)^{3H} (2\pi)^{H+1} \Big( \prod_{\langle x_i, x_j \rangle} \int_0^{2\pi} d\varphi_{x_i x_j} f_{2\pi}(\varphi_{x_i x_j}) \Big) \delta_{2\pi}^{W_x}(\varphi_{x_{k_1} x_{k_2}} + \cdots + \varphi_{x_{k_{2n}} x_{k_1}}) \delta_{2\pi}^{W_y}(\varphi_{x_{q_1} x_{q_2}} + \cdots + \varphi_{x_{q_{2n}} x_{q_1}}) \times \\ &\prod_{\substack{\hexagon \in \mathrm{DG}. \\ \tilde{x} \notin \hexagon}} \delta_{2\pi}(\varphi_{x_i x_{j_1}} + \varphi_{x_i x_{j_2}} + \varphi_{x_i x_{j_3}} + \varphi_{x_i x_{j_4}} + \varphi_{x_i x_{j_5}} + \varphi_{x_i x_{j_6}}). \end{aligned} \tag{5.10}$$

This last expression needs some explanation. In step 2 we ended up with a height model on a triangular lattice. By dualizing this model we introduced dual variables $\varphi_{x_i x_j} \in [0, 2\pi)$ with the orientation from site $x_i$ to site $x_j$, acting between the integer height variables $h_{x_i}$ and $h_{x_j}$.
If we regard $\varphi_{x_i x_j}$ as a current flowing along the bond between site $x_i$ and $x_j$, the constraint in Equation (5.10) suggests that the current is conserved at each site and hence the field is free of

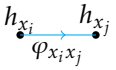


**Figure 5.3:** Orientation bonds.

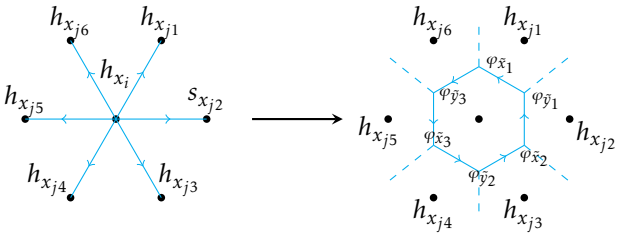


**Figure 5.4:** Rotate dual bonds by 90 degrees.

divergence. The two boundary conditions also turn out to become constraints which imply that the overall current on the torus is conserved, i.e., the total current flowing in the horizontal or vertical direction is 0.
In order to satisfy the constraints, we rotate an arrow of the original dual bond by 90 degrees and define the dual variables $\varphi_{\tilde{x}}$ which reside at both ends of the arrow (see Figure 5.4). As a result, all constraints are satisfied. Starting with

$$Z = (\frac{1}{2\pi})^{3H}(2\pi)^{H+1}(\prod_{\langle x_i,x_j\rangle}\int_0^{2\pi} d\varphi_{x_i x_j} f_{2\pi}(\varphi_{x_i x_j}))\delta_{2\pi}^{W_x}(\varphi_{x_{k_1}x_{k_2}}+\cdots+\varphi_{x_{k_{2n}}x_{k_1}})\delta_{2\pi}^{W_y}(\varphi_{x_{q_1}x_{q_2}}+\cdots+\varphi_{x_{q_{2n}}x_{q_1}})\times$$
$$\prod_{\substack{\hexagon\in DG.\\ \tilde{x}\notin\hexagon}}\delta_{2\pi}(\varphi_{x_i x_{j_1}}+\varphi_{x_i x_{j_2}}+\varphi_{x_i x_{j_3}}+\varphi_{x_i x_{j_4}}+\varphi_{x_i x_{j_5}}+\varphi_{x_i x_{j_6}}),$$

and performing a change of variables (i.e. integrating over dual variables $\varphi_{\tilde{x}}$ instead of dual bonds $\varphi_{x_i x_j}$), we end up with

$$\begin{aligned} Z &= (\frac{1}{2\pi})^{3H}(2\pi)^{H+1}(\prod_{\tilde{x}\in DA_\bullet}\int_0^{2\pi} d\varphi_{\tilde{x}})(\prod_{\tilde{y}\in DB_\circ}\int_0^{2\pi} d\varphi_{\tilde{y}})\frac{1}{2\pi}\prod_{\langle\tilde{x},\tilde{y}\rangle} f_{2\pi}(\varphi_{\tilde{y}}-\varphi_{\tilde{x}}) \\ &= (\frac{1}{2\pi})^{2H}(\prod_{\tilde{x}\in DA_\bullet}\int_0^{2\pi} d\varphi_{\tilde{x}})(\prod_{\tilde{y}\in DB_\circ}\int_0^{2\pi} d\varphi_{\tilde{y}})\prod_{\langle\tilde{x},\tilde{y}\rangle} f_{2\pi}(\varphi_{\tilde{y}}-\varphi_{\tilde{x}}). \end{aligned} \tag{5.11}$$

At this point, we obtain the dualized $\tilde{F}_\Delta$ model at coupling $K = 0$, which is a generalized XY model on a honeycomb lattice. The coordinates of the dual lattice are denoted by $\tilde{x}$ and $\tilde{y}$. On each lattice site, instead of an integer-valued height variable $h_x \in \mathbb{Z}$, we now have an angle $\varphi_{\tilde{x}} \in [0, 2\pi)$, and the nearest-neighbor interaction term is given by

$$f_{2\pi}(\varphi_{\tilde{y}}-\varphi_{\tilde{x}}) = \sqrt[3]{2}(1+\sqrt{2}\cos(2(\varphi_{\tilde{y}}-\varphi_{\tilde{x}})). \tag{5.12}$$

The interaction term $f_{2\pi}(\varphi_{\tilde{y}}-\varphi_{\tilde{x}})$ can become negative, which means that some configurations that contribute to the partition function have negative weight. Hence, the dualized $\tilde{F}_\Delta$ model suffers from a severe sign problem, which prevents numerical simulations. In Equation (5.11), we emphasize once again that the honeycomb lattice is bipartite. Therefore we can split up the integration into an integration over all angles on the $A_\bullet$-dual lattice and an integration over all angles of the $B_\circ$-dual lattice. Note that this model has a $U(1)$ symmetry. We can rotate every angle by a fixed constant $\hat{\varphi}$, and the Hamiltonian stays invariant

$$\begin{aligned} &\varphi_x \to \varphi_x + \hat{\varphi}, \hat{\varphi} \in [0, 2\pi), \forall x \\ \implies &\mathcal{H}[\varphi] \to \mathcal{H}'[\varphi] = \mathcal{H}[\varphi]. \end{aligned} \tag{5.13}$$

Due to the presence of this continuous symmetry, the Mermin-Wagner theorem applies and we can not have a completely ordered phase with continuous symmetry breaking. The previously introduced winding numbers $(W_x, W_y)$ are still present but are hidden in the $2\pi$-periodicity of the

model. The situation is that neighboring parallelograms in $\hat{\mathbf{x}}$ or $\hat{\mathbf{y}}$ direction may differ from the original one by a multiple of $2\pi$ such that

$$\begin{aligned}\varphi_{\tilde{x}+L,\tilde{y}} &= \varphi_{\tilde{x},\tilde{y}} + 2\pi\tilde{W}_y,\\ \varphi_{\tilde{x},\tilde{y}+L} &= \varphi_{\tilde{x},\tilde{y}} + 2\pi\tilde{W}_x.\end{aligned} \tag{5.14}$$

Since we did not introduce twisted boundary conditions, the partition function has no dependence on a twist angle $\alpha$ (see Subsection 2.6.5).

### 5.3.4 Step 4)

Similar to the second step, we now take advantage of the fact that the dualized $\tilde{F}_\Delta$ model lives on a honeycomb lattice which is bipartite. Hence, we can integrate out the angles on the $B_\circ$ sublattice and express the partition function as function of angles on the $A_\bullet$ sublattice only. Since

$$\begin{aligned}\int_0^{2\pi}\Big(\prod_{i=1,2,3} f_{2\pi}(\varphi_{\tilde{y}}-\varphi_{\tilde{x}_i})\Big)d\varphi_{\tilde{y}} &= (16\pi)\cos(\varphi_{\tilde{x}_3}-\varphi_{\tilde{x}_2})\cos(\varphi_{\tilde{x}_2}-\varphi_{\tilde{x}_1})\cos(\varphi_{\tilde{x}_1}-\varphi_{\tilde{x}_3})\\ &= (2\pi)\tilde{b}(\varphi_{\tilde{x}_3}-\varphi_{\tilde{x}_2})\tilde{b}(\varphi_{\tilde{x}_2}-\varphi_{\tilde{x}_1})\tilde{b}(\varphi_{\tilde{x}_1}-\varphi_{\tilde{x}_3}),\end{aligned}$$

we can successfully execute the integration and obtain

$$Z = \Big(\frac{1}{2\pi}\Big)^H\Big(\prod_{\tilde{x}\in \mathrm{D}A_\bullet}\int_0^{2\pi} d\varphi_{\tilde{x}}\Big)\prod_{\langle\tilde{x}_i,\tilde{x}_j\rangle}\tilde{b}(\varphi_{\tilde{x}_j}-\varphi_{\tilde{x}_i}), \tag{5.15}$$

with

$$\tilde{b}(\varphi_{\tilde{x}_j}-\varphi_{\tilde{x}_i}) = 2\cos(\varphi_{\tilde{x}_j}-\varphi_{\tilde{x}_i}). \tag{5.16}$$

We are left with a generalized form of an XY model on a triangular lattice, which is still suffering from a sign problem.

### 5.3.5 Step 5)

Finally, there is only one step left in order to return back to our starting point. Starting from Equation (5.15), we can use the fact that the interaction term $\tilde{b}$ is $2\pi$-periodic and can be written as a Fourier expansion (see appendix A.1), such that

$$\tilde{b}(\varphi_{\tilde{x}_j}-\varphi_{\tilde{x}_i}) = \sum_{h_{\tilde{x}_i\tilde{x}_j}\in\mathbb{Z}} u(h_{\tilde{x}_i\tilde{x}_j})e^{ih_{\tilde{x}_i\tilde{x}_j}(\varphi_{\tilde{x}_j}-\varphi_{\tilde{x}_i})}, \tag{5.17}$$

where the integer-valued variable $h_{\tilde{x}_i\tilde{x}_j}$ can be considered a dual bond (of the dual variable) between $\varphi_{\tilde{x}_j}$ and $\varphi_{\tilde{x}_i}$ with the orientation from site $\tilde{x}_i$ to site $\tilde{x}_j$. For the purpose of avoiding confusion, we refer to $h_{\tilde{x}_i\tilde{x}_j}$ as just the bond variable. We chose to label the Fourier coefficient $u$, since it will turn out to be the interaction term introduced in Equation (5.1). Then the partition function reads

$$\begin{aligned}Z &= \Big(\frac{1}{2\pi}\Big)^H\Big(\prod_{\tilde{x}\in \mathrm{D}A_\bullet}\int_0^{2\pi} d\varphi_{\tilde{x}}\Big)\prod_{\langle\tilde{x},\tilde{y}\rangle}\tilde{b}(\varphi_{\tilde{x}_j}-\varphi_{\tilde{x}_i})\\ &= \Big(\frac{1}{2\pi}\Big)^H\Big(\prod_{\langle\tilde{x}_i,\tilde{x}_j\rangle}\sum_{h_{\tilde{x}_i\tilde{x}_j}\in\mathbb{Z}} u(h_{\tilde{x}_i\tilde{x}_j})\Big)\Big(\prod_{\tilde{x}\in \mathrm{D}A_\bullet}\int_0^{2\pi} d\varphi_{\tilde{x}}\Big)\prod_{\langle\tilde{x}_i,\tilde{x}_j\rangle} e^{ih_{\tilde{x}_i\tilde{x}_j}(\varphi_{\tilde{x}_j}-\varphi_{\tilde{x}_i})}.\end{aligned} \tag{5.18}$$

At this point we need to consider the $2\pi$-periodicity of the boundaries ($\tilde{W}_x, \tilde{W}_y$ as described in step 3) and sum over them

$$Z = \Big(\frac{1}{2\pi}\Big)^H\sum_{\tilde{W}_x\in\mathbb{Z}}\sum_{\tilde{W}_y\in\mathbb{Z}}\Big(\prod_{\langle\tilde{x}_i,\tilde{x}_j\rangle}\sum_{h_{\tilde{x}_i\tilde{x}_j}\in\mathbb{Z}} u(h_{\tilde{x}_i\tilde{x}_j})\Big)\Big(\prod_{\tilde{x}\in \mathrm{D}A_\bullet}\int_0^{2\pi} d\varphi_{\tilde{x}}\Big)\tilde{\prod}_{\langle\tilde{x}_i,\tilde{x}_j\rangle} e^{ih_{\tilde{x}_i\tilde{x}_j}(\varphi_{\tilde{x}_j}-\varphi_{\tilde{x}_i})}. \tag{5.19}$$

The product term now takes into account boundaries, since two angle variables connected by a bond on the edge can have a possible shift of $2\pi\tilde{W}_{x,y}$. The evaluation yields

$$Z = (\frac{1}{2\pi})^H \sum_{\tilde{W}_x\in\mathbb{Z}} \sum_{\tilde{W}_y\in\mathbb{Z}} (\prod_{\langle\tilde{x}_i,\tilde{x}_j\rangle} \sum_{h_{\tilde{x}_i\tilde{x}_j}\in\mathbb{Z}} u(h_{\tilde{x}_i\tilde{x}_j}))(\prod_{\tilde{x}\in \mathrm{D}A_\bullet} \int_0^{2\pi} d\varphi_{\tilde{x}}) \tilde{\prod}_{\langle\tilde{x}_i,\tilde{x}_j\rangle} e^{ih_{\tilde{x}_i\tilde{x}_j}(\varphi_{\tilde{x}_j}-\varphi_{\tilde{x}_i})} \tag{5.20}$$

$$= \sum_{\tilde{W}_x\in\mathbb{Z}} \sum_{\tilde{W}_y\in\mathbb{Z}} (\frac{1}{2\pi})^H (2\pi)^H (\prod_{\langle\tilde{x}_i,\tilde{x}_j\rangle} \sum_{h_{\tilde{x}_i\tilde{x}_j}\in\mathbb{Z}} u(h_{\tilde{x}_i\tilde{x}_j}))\left(\prod_{\hexagon\in \mathrm{DG}.} \delta_{\sum h_{\tilde{x}_i\tilde{x}_j},0}\right) e^{2\pi i\tilde{W}_x(\Sigma\uparrow)} e^{2\pi i\tilde{W}_y(\Sigma\rightarrow)} \tag{5.21}$$

$$= (\frac{1}{2\pi})^H (2\pi)^H (\prod_{\langle\tilde{x}_i,\tilde{x}_j\rangle} \sum_{h_{\tilde{x}_i\tilde{x}_j}\in\mathbb{Z}} u(h_{\tilde{x}_i\tilde{x}_j}))\left(\prod_{\hexagon\in \mathrm{DG}.} \delta_{\sum h_{\tilde{x}_i\tilde{x}_j},0}\right) \delta_1(\Sigma\uparrow)\delta_1(\Sigma\rightarrow) \tag{5.22}$$

$$= \sum_{W_x\in\mathbb{Z}} \sum_{W_y\in\mathbb{Z}} (\prod_{\langle\tilde{x}_i,\tilde{x}_j\rangle} \sum_{h_{\tilde{x}_i\tilde{x}_j}\in\mathbb{Z}} u(h_{\tilde{x}_i\tilde{x}_j}))\left(\prod_{\hexagon\in \mathrm{DG}.} \delta_{\sum h_{\tilde{x}_i\tilde{x}_j},0}\right) \delta(\Sigma\uparrow - W_x)\delta(\Sigma\rightarrow - W_y). \tag{5.23}$$

In the previous equation we used expressions like $\Sigma\uparrow$, which indicate the sum over all bond variables $h_{\tilde{x}_i\tilde{x}_j}$ at one boundary in one direction. One can also interpret this as an integer-valued flow between neighboring parallelograms, leading to the initially introduced winding numbers $(W_x, W_y)$. Evaluating the integrals over the angles $\varphi$, we obtain once again constraints on the hexagons. These can be interpreted in the same way as in step 3) with the only difference that the flow is now integer-valued. One of the constraints given in Equation (5.23) is identically satisfied, so we can get rid of one.

At this point we reintroduce the original integer-valued height variables $h_x$, which are then identically satisfying the imposed constraints. This is done in the same fashion as before: We rotate the bonds in a consistent way by an angle of 90 degree and put integer height variables at the ends of the rotated bonds, such that

$$h_{\tilde{x}_i\tilde{x}_j} = h_y - h_x. \tag{5.24}$$

These new height variables are now living on the original honeycomb lattice we started with. In the end we also need to modify the partition function properly in order to take into account the winding numbers $W_x$ and $W_y$. Since we neglected one constraint we are now free to fix one arbitrary height variable $h_x$, which we choose to be $h_{\tilde{x}}$. We close this loop of transformations ending up with the partition function that we started with

$$Z = \sum_{W_x\in\mathbb{Z}} \sum_{W_y\in\mathbb{Z}} (\prod_{\substack{x\in A_\bullet \\ x\neq\tilde{x}}} \sum_{h_x\in\mathbb{Z}})(\prod_{x\in B_\circ} \sum_{h_y\in\mathbb{Z}}) \tilde{\prod}_{\langle x,y\rangle} u(h_y - h_x). \tag{5.25}$$

# 6 Algorithm for the $\tilde{F}_\Delta$ Model

In Chapter 5 we defined the $\tilde{F}_\Delta$ model, derived some of its properties and revealed that simulating the dualized $\tilde{F}_\Delta$ model on the honeycomb lattice was no option due to the sign problem. Thus what we finally end up simulating is the $\tilde{F}_\Delta$ model with the partition function given by

$$Z(K) = \sum_{W_x\in\mathbb{Z}} \sum_{W_y\in\mathbb{Z}} \Big(\prod_{\substack{x\in A_\bullet \\ x\neq\tilde{x}}} \sum_{h_x\in\mathbb{Z}}\Big)\Big(\prod_{x\in B_\circ} \sum_{h_y\in\mathbb{Z}}\Big)\left(\tilde{\prod_{\langle x,y\rangle}} u(h_y - h_x)\right) \exp\left(-\beta\mathcal{H}[\mathrm{h}]\right), \tag{6.1}$$

where

$$\beta\mathcal{H}[\mathrm{h}] = \frac{K}{4}\sum_{[i,j]}(h_i - h_j)^2 = \frac{K}{4}\left(\sum_{[x_i,x_j]}(h_{x_i} - h_{x_j})^2 + \sum_{[y_i,y_j]}(h_{y_i} - h_{y_j})^2\right). \tag{6.2}$$

The Hamiltonian allows for next-nearest-neighbor interaction on each sublattice, such that we can split up the Hamiltonian into a piece for the $A_\bullet$ sublattice and a piece for the $B_\circ$ sublattice. On each site $x \in A_\bullet$ and $y \in B_\circ$ there is an integer-valued height variable $h_x, h_y \in \mathbb{Z}$ and nearest-neighbors differ by $\pm 1$. We require an algorithm which takes into account the overall shift symmetry of the system, since measurable quantities only depend on height differences. These can be represented by arrows, pointing in the direction of the increasing height variable. We can fix $h_{\tilde{x}} = 0$ in advance to get rid of the $\mathbb{Z}$ symmetry, but we can recover every $h_x \in \mathbb{Z}$ and $h_y \in \mathbb{Z}$ by following the arrows (see Figure 6.1). In order to simulate the $\tilde{F}_\Delta$ model we want to develop a shift-invariant formulation which we will denote as modulo 4 formulation.

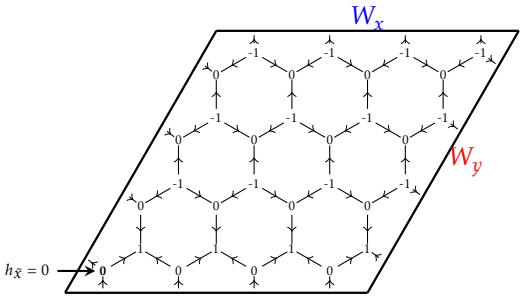


**Figure 6.1:** Possible configuration of height variables: All the other height values can be derived from $h_{\tilde{x}} = 0$.

## 6.1 The Modulo 4 Formulation of the $\tilde{F}_\Delta$ Model

The modulo 4 formulation incorporates the $\mathbb{Z}$ symmetry of the $\tilde{F}_\Delta$ model and allows a straightforward implementation on a computer. Consider the honeycomb lattice where vertices can take values in $\mathbb{Z}_4 = \{0,1,2,3\}$. Due to the bipartite structure of the honeycomb lattice and the constraints of the $\tilde{F}_\Delta$ model we can split up $\mathbb{Z}_4$ into an even and an odd part such that for $x \in A_\bullet$ and $y \in B_\circ$ we have

$$h_x \in \{0,2\}, \qquad\qquad h_y \in \{1,3\}.$$

The assignment of the ±1 steps between nearest-neighbors is illustrated in Figure 6.2. This formulation also allows the construction of hexagons which are forbidden in the original $\tilde{F}_\Delta$ model formulation as illustrated in Figure 6.3. The general rule is that the sum of positive and negative steps around a hexagon must be 0.

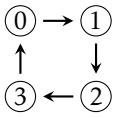


**Figure 6.2:** Step ±1 assignments on links.

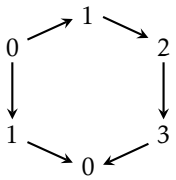


**Figure 6.3:** Forbidden hexagon configuration.

### 6.1.1 Constraint Cluster Rules at Coupling $K = 0$

Up to this point we associated a height variable $h_x, h_y \in \mathbb{Z}_4$ with each vertex of the lattice. In order to construct an algorithm, we need to develop a cluster building prescription. Let us first consider the case where the coupling $K$ is zero, which implies that we are only building up constraint clusters. The $\tilde{F}_\Delta$ model belongs to the class of height models, so we are reminded of a landscape with mountains and valleys. Clusters are then built by taking one sublattice first (e.g. the $B_\circ$ sublattice) and building closed loops of the same height, so-called contour lines. In our current modulo 4 formulation we flatten out the mountains and valleys and remain with a landscape where heights only take values $h_x, h_y \in \{0, 1, 2, 3\}$. Nonetheless, we can identify clusters in a unique manner; they now divide areas of different heights on the other sublattice.

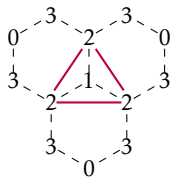


**Figure 6.4:** Cluster of the $B_\circ$ sublattice separating two different regions of the other sublattice.

In Figure 6.4 we consider a fraction of the honeycomb lattice. Assume that we wanted to update the $A_\bullet$ sublattice and construct clusters on it. The triangle (in purple) of height 2 sites, separates the region of the height 1 site (in the middle) and the height 3 sites outside the contour line. Single-site clusters are the ones where the three nearest-neighboring height variables $h_{x_1}, h_{x_2}, h_{x_3}$ have the same value (in Figure 6.4 we have such a case, where the cluster in the middle is a single-site cluster). After all the clusters of the $A_\bullet$ sublattice are built, each of them is flipped with probability 50% (including single-site clusters).
The flipping prescription is straightforward, since for each sublattice there are only two different options. A height variable on the $A_\bullet$ sublattice only has values $\{0, 2\}$ which are mapped into each other when performing a cluster flip ($0 \mapsto 2, 2 \mapsto 0$). For the $B_\circ$ sublattice, 1 and 3 are mapped into each other. This cluster building and flipping prescription leads to "arrow conservation" for each hexagon, so starting from an allowed configuration, which does not contain any forbidden hexagon configuration (see Figure 6.3), we will never reach a forbidden configuration. This makes the algorithm consistent. Throughout all simulations, we start with an allowed configuration, namely the **reference configuration**, where $h_x = 0\ \forall x \in A_\bullet$ and $h_y = 1\ \forall y \in B_\circ$. One Monte Carlo step is characterized by first updating the $A_\bullet$ sublattice and then the $B_\circ$ sublattice.

### 6.1.2 Boundary Updates

Starting from the reference configuration, we see that the twists which define the boundary conditions for that configuration are set to zero, i.e. $W_x = 0$ and $W_y = 0$. When we specified the partition function in Equation (6.1), we summed up all possible sectors characterized by $W_x \in \mathbb{Z}$ and $W_y \in \mathbb{Z}$. Taking into account the structure of the constraints and the geometry of the lattice, we come to realize that, in fact, $W_x, W_y \in 2\mathbb{Z}$. Consequently, the partition function can be split up into different pieces

$$\begin{aligned} Z &= \sum_{\substack{W_x \in 2\mathbb{Z} \\ W_y \in 2\mathbb{Z}}} Z[W_x, W_y] \\ &= \sum_{\substack{W_x \in 4\mathbb{Z} \\ W_y \in 4\mathbb{Z}}} Z[W_x, W_y] + \sum_{\substack{W_x \in 4\mathbb{Z}+2 \\ W_y \in 4\mathbb{Z}}} Z[W_x, W_y] + \sum_{\substack{W_x \in 4\mathbb{Z} \\ W_y \in 4\mathbb{Z}+2}} Z[W_x, W_y] + \sum_{\substack{W_x \in 4\mathbb{Z}+2 \\ W_y \in 4\mathbb{Z}+2}} Z[W_x, W_y]. \end{aligned} \tag{6.3}$$

The split up in the second line is convenient when one considers the effects of cluster updates on the boundary condition. Every allowed configuration [h] belongs to a winding number sector characterized by a boundary twist. Every cluster we build, which has non-trivial winding number (i.e. which wraps around the torus as described in Subsection 4.3.1), changes the corresponding winding number by ±4. The following configuration is the same as in Figure 6.1, but with the modulo 4 formulation applied to it (i.e. every −1 goes to 3).

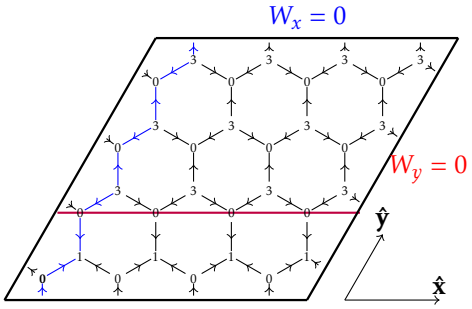


**Figure 6.5:** Parallelogram and cluster.

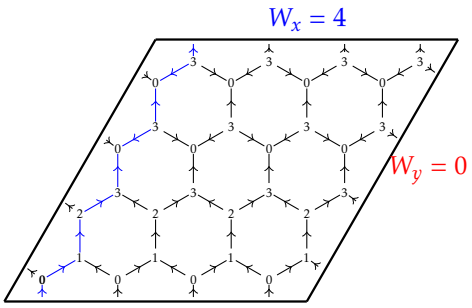


**Figure 6.6:** Parallelogram after flipping.

If we backtrack the original height variables ($h_x, h_y \in \mathbb{Z}$) starting from the fixed one at the bottom left corner, we see that at the boundaries no shifts in height variables are needed such that $h_{x+L,y} = h_{x,y}$ and $h_{x,y+L} = h_{x,y}$, thus $W_x = W_y = 0$. In the modulo 4 formulation, this can also be checked by taking the steps in the horizontal or vertical direction along a closed loop.
Consider the purple cluster on the $A_\bullet$ sublattice in Figure 6.5, which separates a height 1 area and a height 3 area on the $B_\circ$ sublattice. This particular cluster wraps horizontally around the torus, which means that after flipping it, the boundary twist $W_x$ changes. If we flip that cluster, the sum over the vertical arrows along one loop in $\hat{\mathbf{y}}$-direction does not yield 0 but 4, therefore $W_x = 4$.
Starting from the reference configuration, we see that only a fraction of all configurations can be reached, namely the ones where $(W_x, W_y) \mod 4 = (0,0)$ [1]. Since we are not able to dynamically reach all possible winding sectors, the algorithm is not ergodic. However, the algorithm is ergodic in the sense that we can reach every allowed height configuration within the sectors where $(W_x, W_y) \mod 4 = (0,0)$ (see Section 6.2).

[1] compare to Equation (6.3)

### 6.1.3 Next-nearest-neighbor Interaction

Up to this point we just considered the cluster-building prescription for the case $K = 0$ (no coupling). If we turn on $K$, we allow for next-nearest neighbor interactions, which implies that we allow to freeze links with a certain non-vanishing probability $p$. The relation between the coupling $K$ and the bond setting probability $p$, can be established in the same fashion as for the Swendsen-Wang cluster algorithm for the Ising model (see Subsection 3.5.2). Consider two adjacent height variables on the same sublattice which have the same height value $h$. Then the contribution to the partition function can be split up into a part where a link is frozen and a part where no link is set.

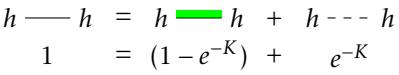


**Figure 6.7:** Bond splitting in the $\tilde{F}_\Delta$ model.

Hence the probability for a bond to be frozen between two sites with the same height value is given by

$$p = 1 - e^{-K} \in [0, 1], \tag{6.4}$$

which provides us with the relation between the coupling $K$ and the bond freezing probability $p$. Throughout this thesis we refer to the bond freezing probability $p$ as the coupling parameter, due to its one-to-one correspondence with the original coupling parameter $K$. When updating the $A_\bullet$ sublattice, we build all clusters which are determined by the constraints and are therefore built by also considering the opposite sublattice. The coupling parameter $p$ acts within one sublattice, freezes certain links and allows for larger clusters. As an example, consider the triangle in Figure 6.9. Assume that the red line divides a height 1 region from a height 3 region, implying that it is part of a constraint cluster. With probability $p$ we set a link $l_1$ respectively a link $l_2$ to the triangle and therefore add the remaining 0 vertex to the cluster.

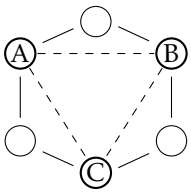


**Figure 6.8:** Triangular lattice within the honeycomb lattice.

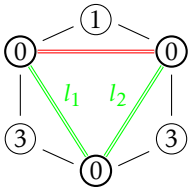


**Figure 6.9:** Possible hexagon.

By investigating the $\tilde{F}_\Delta$ model for different couplings $p$, we will see that we encounter a dual form of the BKT-transition at a certain critical coupling $p_c$.

## 6.2 Detailed Balance and Ergodicity

As discussed in Section 3.4, a Monte Carlo algorithm which obeys ergodicity and detailed balance is guaranteed to converge to the correct equilibrium distribution. Consider an arbitrary initial configuration [h] and another configuration [h′], such that both configurations belong to winding sectors where $(W_x, W_y) \mod 4 = (0, 0)$. In order to prove ergodicity we want to show that we can reach the configuration [h′] in a finite number of Monte Carlo steps such that

$$[\mathrm{h}] \to \ldots \to [\mathrm{h}']. \tag{6.5}$$

This can actually be accomplished in just two steps, by constructing the reference configuration in the first step. First we update the $A_\bullet$ sublattice of the starting configuration [h]. We build

all the clusters of the $A_\bullet$ sublattice and flip every cluster which has the $\mathbb{Z}_4$ variable 2, such that every site on the $A_\bullet$ sublattice now has the height variable 0. Next we consider the $B_\circ$ sublattice, build up the clusters and then flip all clusters which have a height variable of 3. We end up with the reference configuration, where on the $A_\bullet$ sublattice all heights have value 0 and on the $B_\circ$ sublattice all heights have value 1. From this point on we can reach any configuration [h′] (up to an overall shift) by visiting each site in [h] and flipping the height variable if needed. In order to show detailed balance we use the fact that the partition function factorizes, such that it is sufficient to consider two adjacent heights only. In our particular case we work with two adjacent heights on one triangular sublattice, where one of the heights is given by $h_i$ and the other one is given by $h_j \in \{h_i, h_i \pm 2\}$. We denote the situation where both heights are the same by $\uparrow\uparrow$ and the situation where both heights differ by $\uparrow\downarrow$. Then three situations may occur as in the specific case of the Ising ferromagnetic (see Section 3.4).

1. $\uparrow\downarrow \leftrightarrow \uparrow\downarrow$

$$p[\uparrow\downarrow]w[\uparrow\downarrow,\uparrow\downarrow] = p[\uparrow\downarrow]w[\uparrow\downarrow,\uparrow\downarrow]$$

2. $\uparrow\uparrow \leftrightarrow \uparrow\uparrow$

$$p[\uparrow\uparrow]w[\uparrow\uparrow,\uparrow\uparrow] = p[\uparrow\uparrow]w[\uparrow\uparrow,\uparrow\uparrow]$$

3. $\uparrow\downarrow \leftrightarrow \uparrow\uparrow$

$$p[\uparrow\downarrow]w[\uparrow\downarrow,\uparrow\uparrow] = p[\uparrow\uparrow]w[\uparrow\uparrow,\uparrow\downarrow]$$
$$\frac{e^{-K}}{Z(\beta)}\frac{1}{2} = \frac{1}{Z(\beta)}\frac{1}{2}(1-p)$$

As we can see, all three situations satisfy the detailed balance condition. Thus the modulo 4 algorithm applied to the $\tilde{F}_\Delta$ model obeys ergodicity and detailed balance.

## 6.3 The Modulo 4 Formulation and the Ising Model

Having set up the modulo 4 formulation, we recognize the $\mathbb{Z}_4$ symmetry, which can be further reduced to a $\mathbb{Z}_2$ symmetry if we fix an odd and an even sublattice. By considering the even and the odd sublattices independent of each other, we can associate those sublattices to the Ising model on a triangular lattice; this is the way how we measure observables. We make the following assignments

$$\begin{bmatrix}0\\1\\2\\3\end{bmatrix} \mapsto \begin{bmatrix}-1\\-1\\1\\1\end{bmatrix},$$

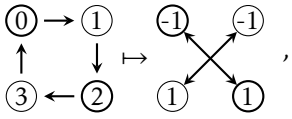


**Figure 6.10:** New assigments for variables.

which provides us with a well-defined way of measuring observable quantities. Note, that after making these assignments, it does not make sense to calculate combined observables on the entire hexagonal lattice, since we assigned the ±1 measurement values to both sublattices in an ambiguous way.
For instance, when defining observables $\langle\mathcal{O}\rangle$, we measure them for each sublattice such that

$$\langle\mathcal{O}\rangle = \langle\mathcal{O}_A + \mathcal{O}_B\rangle. \tag{6.6}$$

As an example, $\mathcal{M}^2$ takes the form $\langle\mathcal{M}^2\rangle = \langle\mathcal{M}_A^2 + \mathcal{M}_B^2\rangle$.

## 6.4 Improved Estimators

We already mentioned that, due to the applied formalism, we need to take into account both sublattices separately, i.e., if not mentioned otherwise, we have

$$\langle \mathcal{O} \rangle = \langle \mathcal{O}_A + \mathcal{O}_B \rangle. \tag{6.7}$$

Two interesting observables we want to measure are the magnetization $\mathcal{M}$ and the winding number $W_x$. We expect $\langle \mathcal{M} \rangle = 0$ and $\langle W_x \rangle = 0$ (One should keep in mind that for the measurement we have $h_x, h_y \in \{-1, 1\}$), but $\mathcal{M}^2$ and $W_x^2$ contain non-trivial interesting information about the system. The magnetization is

$$\begin{aligned} \langle \mathcal{M} \rangle &= \langle \mathcal{M}_A + \mathcal{M}_B \rangle \\ &= \langle \sum_{x \in A_\bullet} h_x + \sum_{x \in B_\circ} h_y \rangle, \end{aligned} \tag{6.8}$$

and the winding number is

$$\langle W_x \rangle = \langle \sum \uparrow \rangle. \tag{6.9}$$

In the previous equation $\sum \uparrow$ denotes the sum over all up-going arrows minus the sum over all down-going arrows in the vertical direction belonging to one closed loop on the lattice (compare with the blue arrows in Figure 6.5 and in Figure 6.6).
Generally it is possible to employ different methods to calculate some physical quantity. Some of these methods may be more efficient in terms of computational time and have less fluctuations than others. It is often convenient to express measurable quantities in terms of clusters and use these expressions in order to compute observables. We now construct improved estimators for the magnetization $\mathcal{M}$ and the winding number $W_x$. For the sublattice $A_\bullet$ we write

$$\langle \mathcal{M}_A \rangle = \langle \sum_{x \in A_\bullet} s_x \rangle = \langle \sum_{\mathcal{C}} \mathcal{M}_\mathcal{C} \rangle = \langle \sum_{\mathcal{C}} \text{sign}(\mathcal{M}_\mathcal{C}) |\mathcal{M}_\mathcal{C}| \rangle = 0, \tag{6.10}$$

where $\mathcal{M}_\mathcal{C}$ denotes the total height value of a cluster and $|\mathcal{M}_\mathcal{C}|$ is the size of the cluster. For $\mathcal{M}_A^2$ we then obtain

$$\begin{aligned} \langle \mathcal{M}_A^2 \rangle &= \sum_{\mathcal{C}_1} \sum_{\mathcal{C}_2} \langle \text{sign}(\mathcal{M}_{\mathcal{C}_1}) |\mathcal{M}_{\mathcal{C}_1}| \text{sign}(\mathcal{M}_{\mathcal{C}_2}) |\mathcal{M}_{\mathcal{C}_2}| \rangle \\ &= \langle \sum_{\mathcal{C}} |\mathcal{M}_\mathcal{C}|^2 \rangle. \end{aligned} \tag{6.11}$$

The computation of $\mathcal{M}_A^4$ is also straightforward

$$\begin{aligned} \langle \mathcal{M}_A^4 \rangle &= \sum_{\mathcal{C}_1} \sum_{\mathcal{C}_2} \sum_{\mathcal{C}_3} \sum_{\mathcal{C}_4} \langle \mathcal{M}_{\mathcal{C}_1} \mathcal{M}_{\mathcal{C}_2} \mathcal{M}_{\mathcal{C}_3} \mathcal{M}_{\mathcal{C}_4} \rangle, \\ &= 3 \sum_{\mathcal{C}_1} \sum_{\mathcal{C}_2} \langle \mathcal{M}_{\mathcal{C}_1}^2 \mathcal{M}_{\mathcal{C}_2}^2 \rangle - 2 \sum_{\mathcal{C}} \langle \mathcal{M}_\mathcal{C}^4 \rangle. \end{aligned} \tag{6.12}$$

We also find improved estimators for the winding number $\langle W_x \rangle$ and $\langle W_x^2 \rangle$. It is sufficient to calculate one winding number since $\langle W_y \rangle$ and $\langle W_y^2 \rangle$ behave in the same way. The remaining winding number (let's call it $W_z$) is determined by the other ones

$$W_x + W_y + W_z = 0.$$

We already know that each cluster with non-trivial winding number has an effect of $\pm 4$ on the winding number when flipped. Since a cluster is flipped with probability 50%, we conclude that

the overall effect of a cluster with non-trivial winding number is given by $W_{\mathcal{C}} = \pm 2$, such that we obtain

$$\langle W_x \rangle = \langle \sum \uparrow \rangle = \langle \sum_{\mathcal{C}} W_{\mathcal{C}} \rangle = 0,$$
$$\langle W_x^2 \rangle = \sum_{\mathcal{C}_1} \sum_{\mathcal{C}_2} \langle W_{\mathcal{C}_1} W_{\mathcal{C}_2} \rangle = \langle \sum_{\mathcal{C}} W_{\mathcal{C}}^2 \rangle.$$

## 6.5 Autocorrelation Effects

Previously we described the algorithm which will be used throughout this thesis. As described in Chapter 3, we take into account the thermalization procedure and the autocorrelation time. In order to take into account the initial thermalization we dismiss the first 200'000 iterations and then execute $N = 2'000'000$ sweeps for the averaging. The lattice sizes we take into account are

$$L \in \{16, 32, 64, 96, 128, 160, 192, 256, 320, 384, 448, 512\}. \tag{6.13}$$

Since each lattice has two sublattices the total number of height variables is given by $2L^2$. In order to take into account autocorrelation effects between subsequently generated configurations, we perform a binning procedure. The idea behind this procedure is to divide subsequently generated measurements into sufficiently large bins, average all measurements of a bin, and then consider the bin averages as independently generated measurements. Concretely, let us create $m$-sized bins of subsequently generated measurement values, where $m$ is a divisor of $N = 2'000'000$, such that we obtain $n = N/m$ bins

$$\underbrace{\mathcal{O}[\mathrm{h}^{(1)}], ..., \mathcal{O}[\mathrm{h}^{(m)}]}_{B_1}, \underbrace{\mathcal{O}[\mathrm{h}^{(m+1)}], ..., \mathcal{O}[\mathrm{h}^{(2m)}]}_{B_2}, ..., \underbrace{\mathcal{O}[\mathrm{h}^{((n-1)\cdot m+1)}], \cdots, \mathcal{O}[\mathrm{h}^{(N=n\cdot m)}]}_{B_n}. \tag{6.14}$$

Each of these $n$ bins gets averaged and is representing a measurement of an observable $\mathcal{O}$. Assuming that subsequently generated bins are independent of each other the variance is given by

$$\Delta\mathcal{O}(n)^2 = \frac{1}{n(n-1)} \sum_{i=1}^{n} (B_i - \overline{B})^2, \tag{6.15}$$

where

$$B_i = \frac{1}{m} \sum_{k=(i-1)\cdot m+1}^{i\cdot m} \mathcal{O}[\mathrm{h}^{(k)}], \tag{6.16}$$

and

$$\overline{B} = \frac{1}{n} \sum_{i=1}^{n} B_i = \overline{\mathcal{O}}. \tag{6.17}$$

With increasing bin size $m$, the error $\Delta\mathcal{O}(n)^2$ increases until it reaches a plateau (see Figure 6.11) and stabilizes. The stabilized error represents a reliable estimate for the variance $\Delta\mathcal{O}^2$. If the bin size $m$ is 1 we obtain the naive error estimate described in Equation 3.6. After reaching the plateau, fluctuations arise due to the very small number of independent measurements. We compute $\Delta\mathcal{O}(n)^2$ for different bin sizes $m$, different couplings and different observables $\mathcal{O}$. By doing this we determine the characteristic bin size $m$, where the error $\Delta\mathcal{O}(n = N/m)^2$ stabilizes and obtain a reliable estimate for the standard deviation.

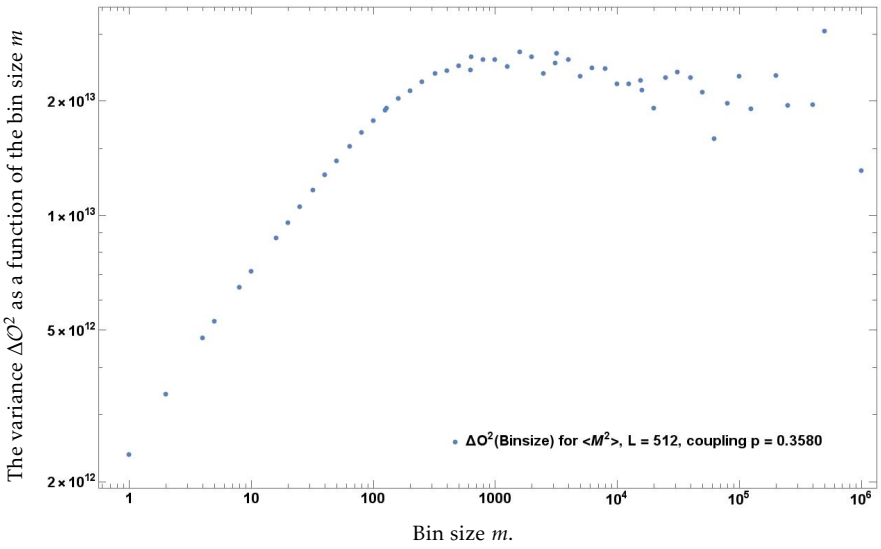


**Figure 6.11:** Evolution of the error during the binning procedure. We see that the error on $\langle \mathcal{M}^2 \rangle$ stabilizes at bin size $m \approx 1000$.

## 6.6 Jackknife Method for the Binder Cumulant

In the previous subsection we described how to properly perform the error analysis for subsequently generated observables. However, a non-linear combination of such observables may still lead to problems. Consider, for example, the Binder cumulant defined as

$$U_4 = \frac{\langle \mathcal{M}_A^4 + \mathcal{M}_B^4 \rangle}{\langle (\mathcal{M}_A^2 + \mathcal{M}_B^2) \rangle^2}. \tag{6.18}$$

For each configuration [h] the denominator is related to the numerator. In order to diminish correlation effects between the denominator and the numerator we want to average as many observables as possible for $\langle \mathcal{M}^4 \rangle$ and $\langle \mathcal{M}^2 \rangle$ and then compute $U_4$. Assume that we have performed the binning procedure described previously and the observables $\mathcal{M}^4$ and $\mathcal{M}^2$ are binned such that we have measurements $(\mathcal{M}^4_{B_1}, \mathcal{M}^4_{B_2}, ..., \mathcal{M}^4_{B_n})$ and $(\mathcal{M}^2_{B_1}, \mathcal{M}^2_{B_2}, ..., \mathcal{M}^2_{B_n})$. Then we define the $i-th$ Jackknife replicate as

$$\hat{U}_{(i)} = \frac{\frac{1}{n-1}\sum_{k=1,k\neq i}^{n} \mathcal{M}^4_{B_k}}{\left(\frac{1}{n-1}\sum_{k=1,k\neq i}^{n} \mathcal{M}^2_{B_k}\right)^2}, \tag{6.19}$$

and the empirical average of the Jackknife replicate reads

$$\hat{U}_{(.)} = \frac{1}{n}\sum_{i=1}^{n} \hat{U}_{(i)}. \tag{6.20}$$

Based on this construction we obtain the Jackknife standard error

$$\Delta\mathcal{O}^2_{\text{Jack}} = \frac{n-1}{n}\sum_{i=1}^{n} (\hat{U}_{(i)} - \hat{U}_{(.)})^2, \tag{6.21}$$

which is the standard deviation squared for the Binder cumulant (see [27]).

# 7 Results

## 7.1 Distribution of the Magnetization of both Sublattices

In order to get a first impression on how the magnetizations $\mathcal{M}_A$ and $\mathcal{M}_B$ of the $A_\bullet$ sublattice and the $B_\circ$ sublattice are distributed as a function of $p$, we take a closer look at the observable $(\mathcal{M}_A, \mathcal{M}_B)$ and investigate its distribution. The algorithm was applied to a lattice with $L = 64$ and after 10'000 thermalization sweeps, the magnetizations of both sublattices $(\mathcal{M}_A, \mathcal{M}_B)$ were measured. For the averaging 200'000 sweeps were made and the values of $(\mathcal{M}_A, \mathcal{M}_B)$ were listed into bins.

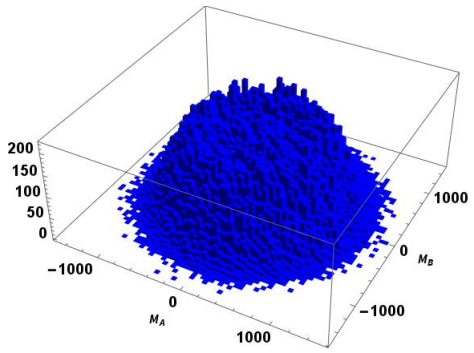


**Figure 7.1:** $(\mathcal{M}_A, \mathcal{M}_B)$ at $p = 0$.

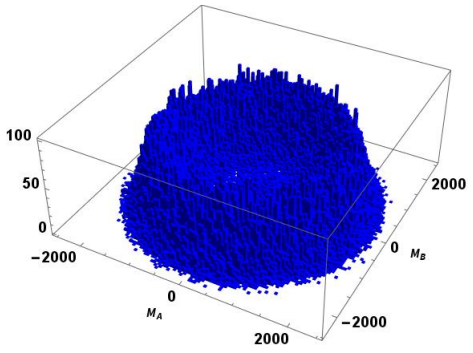


**Figure 7.2:** $(\mathcal{M}_A, \mathcal{M}_B)$ at $p = 0.20$.

As we can see, at $p = 0$ we start with a distribution that is peaked in the middle (Figure 7.1). Since we do not freeze any additional links, only constraint clusters are built which do not lead to configurations where order is predominantly generated. With increasing $p$, more and more bonds are set, which therefore leads to larger clusters. This manifests itself in the fact that the magnetizations $\mathcal{M}_A$ and $\mathcal{M}_B$ of both sublattices become bigger. The peak spreads out, leaving a hole in the middle, which becomes larger with increasing coupling (Figure 7.2). Although the distribution does not form a perfect circle we still see that there is some sort of rotational symmetry in the parameter-space described by $(\mathcal{M}_A, \mathcal{M}_B)$.

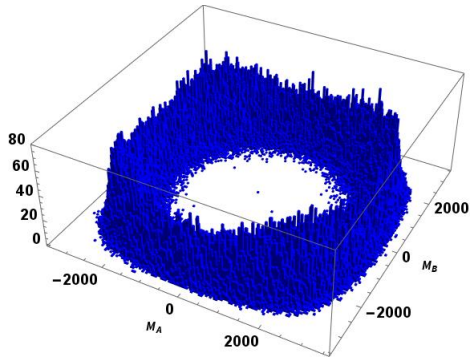


**Figure 7.3:** $(\mathcal{M}_A, \mathcal{M}_B)$ at $p = 0.35$.

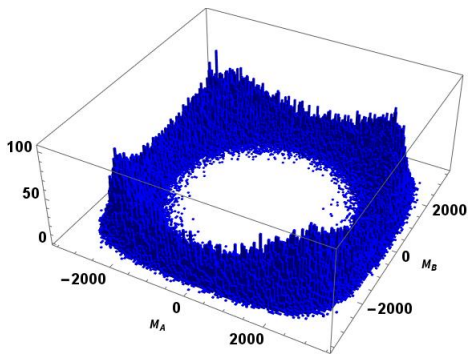


**Figure 7.4:** $(\mathcal{M}_A, \mathcal{M}_B)$ at $p = 0.36$.

For $p \to 0.35$ we see that we are close to a circle, but at $p \approx 0.36$ we also recognize that the rotational symmetry of the observable $(\mathcal{M}_A, \mathcal{M}_B)$ seems to break (see Figure 7.3 and 7.4). At the edges of the distribution four peaks begin to form. This implies that configurations with large magnetization $\mathcal{M}_{A,B}$ appear more often. We are now entering the rigid phase. With increasing coupling $p$ the

peaks are moving to the edges belonging to $(\mathcal{M}_A, \mathcal{M}_B) \in \{(\pm 4096, \pm 4096)\}$, finally leading to total order when the coupling parameter $p$ reaches $p = 1$ (see Figures 7.5 and 7.6).

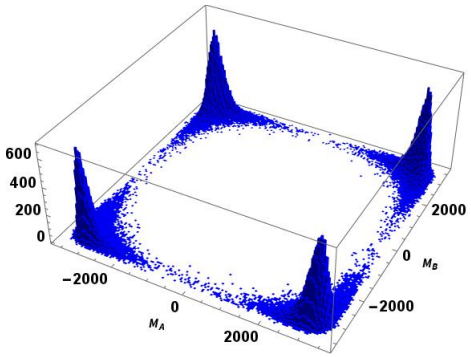


**Figure 7.5:** $(\mathcal{M}_A, \mathcal{M}_B)$ at $p = 0.4$.

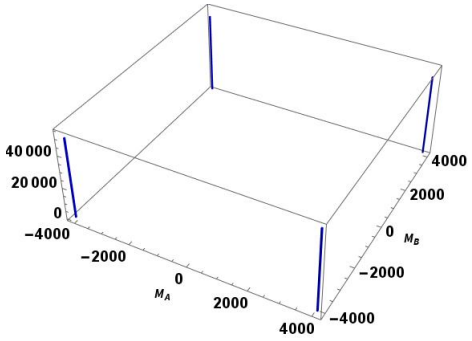


**Figure 7.6:** $(\mathcal{M}_A, \mathcal{M}_B)$ at $p = 1$.

We see that at $p \approx 0.36$, the rotational symmetry of the observable $(\mathcal{M}_A, \mathcal{M}_B)$ breaks and more weight is given to configurations with a large magnetization, which means that we are entering an rigid phase. Therefore $p \approx 0.36$ is a first estimate for the critical coupling $p_c$. The geometrical behavior of $(\mathcal{M}_A, \mathcal{M}_B)$ is very interesting, since starting with a bump in the middle the distribution approximates a circle before breaking up into four pieces.

## 7.2 Susceptibility and Magnetization per Spin

We can confirm this estimation by taking a closer look at the susceptibility and the absolute value of the magnetization per spin

$$\chi = \frac{\langle \mathcal{M}_A^2 + \mathcal{M}_B^2 \rangle}{2L^2}(p), \qquad |\mathcal{M}|_{\text{p.s.}} = \frac{\langle |\mathcal{M}_A| + |\mathcal{M}_B| \rangle}{2L^2}(p). \tag{7.1}$$

As we see in Figures 7.7 and 7.8, there is a fast increase for $\chi$ and $|\mathcal{M}|_{\text{p.s.}}$ at around $p \approx 0.36$. Note that, compared to Figure 2.6, one might expect a much more abrupt increase of $|\mathcal{M}|_{\text{p.s.}}(p)$ at the critical coupling $p_c$. However, one should keep in mind that Figure 2.6 is just the theoretical picture for an infinitely large lattice. Since we can only simulate finite lattices, finite-size effects arise. These smooth out the curves in Figure 7.7 and 7.8, while still approaching the desired behavior for large lattices. As it turns out, we are dealing with a dual form of the BKT-transition separating a rigid (smooth) phase from a rough one.

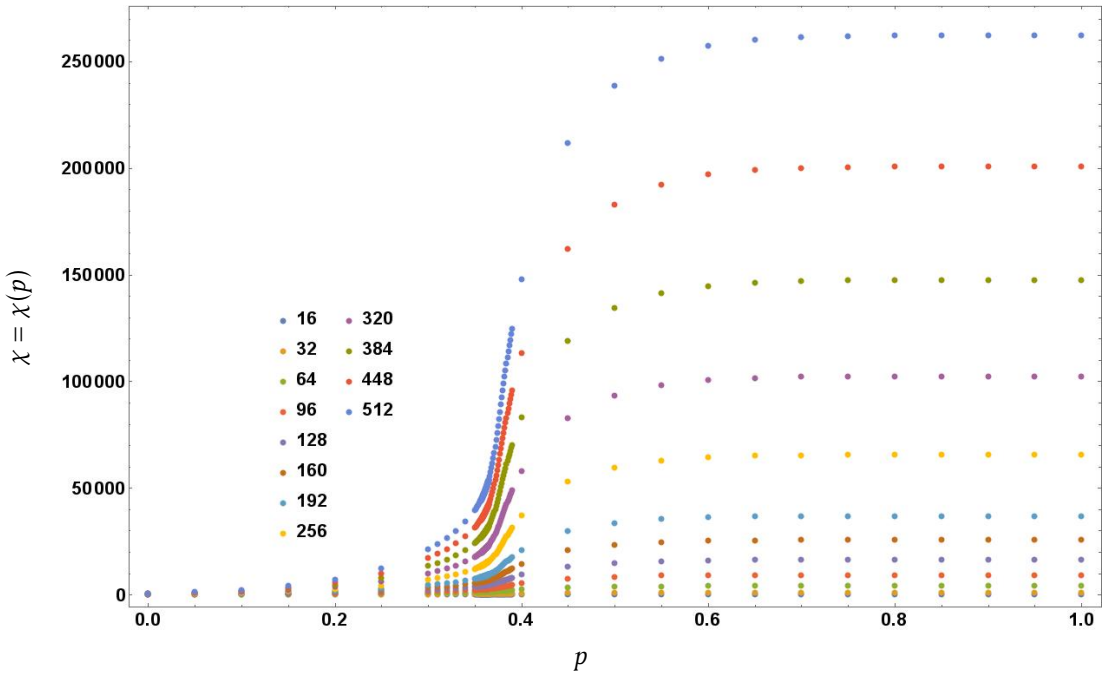


**Figure 7.7:** Susceptibility $\chi(p)$, for different lattice sizes.

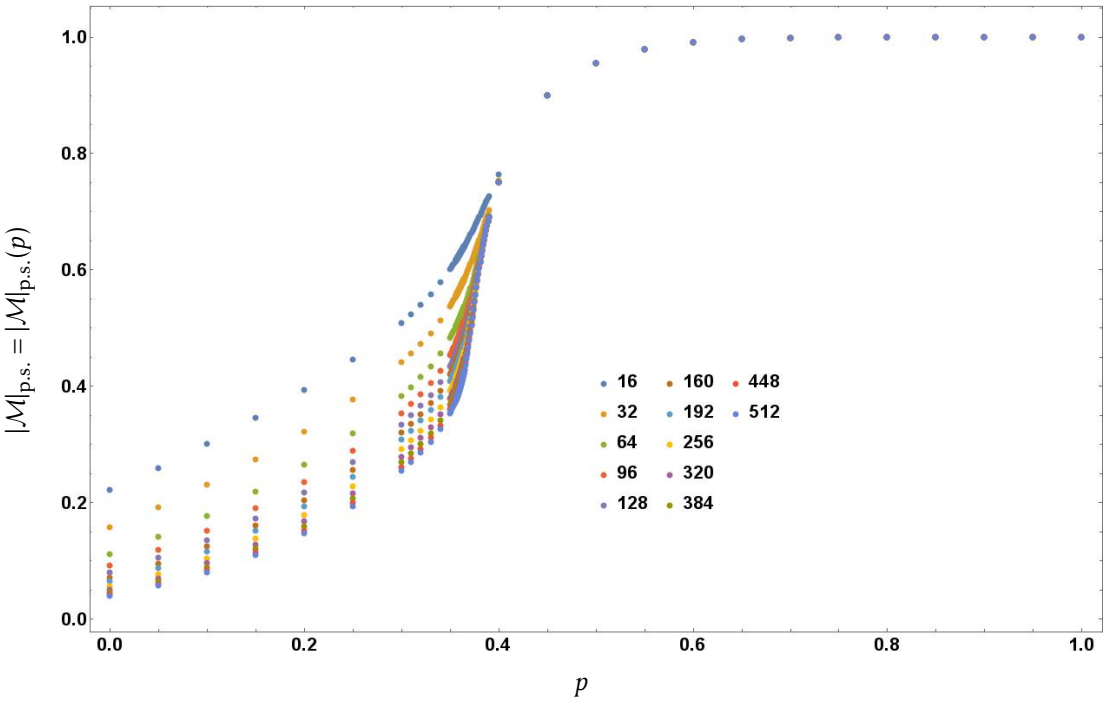


**Figure 7.8:** Absolute value of the magnetization per spin $|\mathcal{M}|_{\text{p.s.}}(p)$, for different lattice sizes.

## 7.3 Correlation Function

The behavior of the correlation function $\Gamma(r)$ for an Ising ferromagnet is described by

$$\Gamma(r) = \langle s_0 s_r \rangle - \langle s_0 \rangle \langle s_r \rangle. \tag{7.2}$$

In Section 6.3 we reduced the $\tilde{F}_\Delta$ model, where on each lattice site we have an integer-valued height variable, to a $\mathbb{Z}$ invariant Ising-type formulation, where $h_x \in \{\pm 1\}$. Hence, we can utilize the same expression for the correlation function (see Equation 7.2) and fit it to the most general form

$$\Gamma(r) = \langle h_0 h_r \rangle - \langle h_0 \rangle \langle h_r \rangle \propto \frac{1}{r^\eta} e^{-\frac{r}{\xi}}, \tag{7.3}$$

for different couplings $p$. Comparing our data with this theoretical model implies that the correlation length is infinite ($\xi = \infty$) for all $p \in [0,1]$. For $p \leq p_c$ we obtain a rough phase with infinite correlation length such that the correlation function behaves as $\Gamma(r) \propto \frac{1}{r^\eta}$. When fitting $\eta$, we want to take into account the long-range contributions from the other side of the finite system, therefore the ansatz is

$$\Gamma(r) \sim c\left(\frac{1}{r^\eta} + \frac{1}{(L-r)^\eta}\right) + d, \tag{7.4}$$

for $p \leq p_c$. For $p > p_c$ we are entering the rigid phase, which indicates that we expect $\Gamma(r)$ to approach a constant, until reaching $\Gamma(r) \to 1$ for $p \to 1$.
In the rigid phase near the critical point we include an exponential correction term to the correlation function, with a second order sub-leading correlation length $\xi^{(2)}$. Therefore the fitting ansatz is given by

$$\Gamma(r) \sim c\left(\frac{e^{\frac{-r}{\xi^{(2)}}}}{r^\eta} + \frac{e^{-\frac{L-r}{\xi^{(2)}}}}{(L-r)^\eta}\right) + d,\ p > p_c, p \approx p_c. \tag{7.5}$$

The exponential term and the power-law term vanish for increasing $p$, indicating that $\eta \to 0$ and $\xi^{(2)} \to \infty$. For increasing coupling the constant $d$ becomes more and more dominant, confirming an infinite correlation (see Figure 7.9).
By analyzing the correlation function we can already draw some conclusions. We have a rough phase with long-range correlation for $p \leq p_c$. This means that throughout this range of couplings the correlation function behaves like

$$\Gamma(r) \propto \frac{1}{r^\eta}, \tag{7.6}$$

where $\eta$ is a continuously varying critical exponent, starting at $\eta(p = 0) \approx 1$ and reaching $\eta(p_c \approx 0.36) \approx 0.25$. For $p > p_c$ we are in a rigid phase, where we have infinite correlation and therefore

$$\Gamma(r) \propto \text{const.} \tag{7.7}$$

Throughout the whole range of couplings $p \in [0,1]$, we could not measure any exponential long-range contributions to the correlation function. Therefore we have an infinite correlation length ($\xi = \infty$) for all couplings $p$.

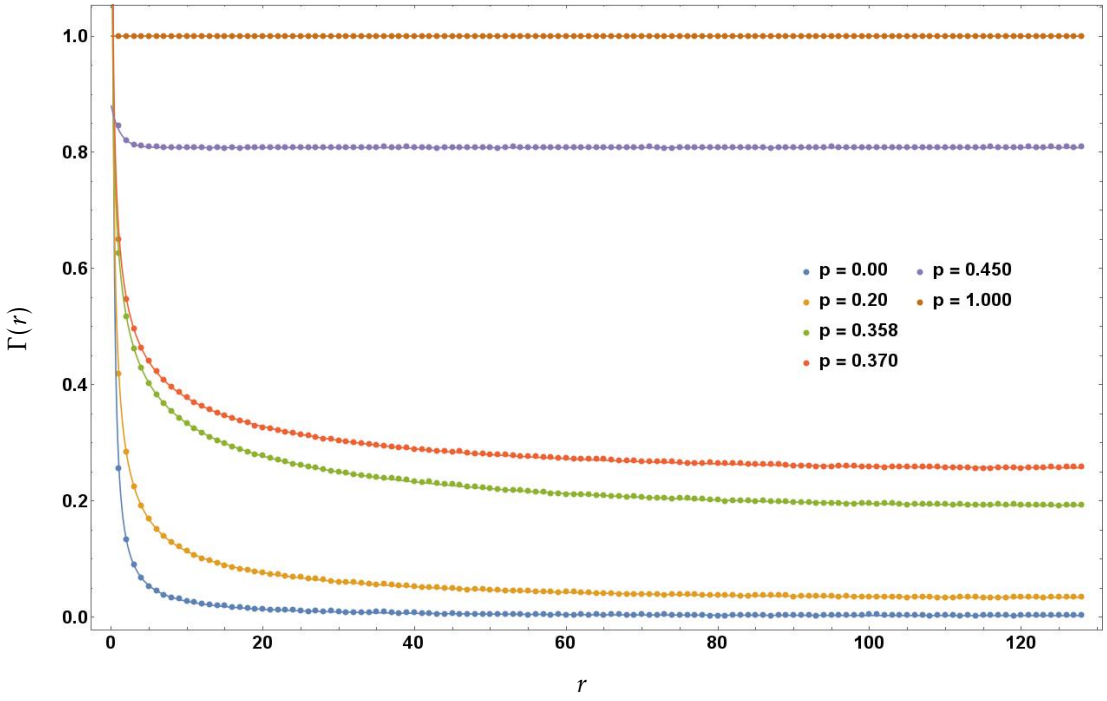


**Figure 7.9:** Correlation function $\Gamma(r)$ for $L = 256$ and different $p$.

## 7.4 Binder Cumulant

Up to this point we estimated the critical coupling $p_c$ visually, without using a quantitative method that provides us with a precise numerical estimate. At this point we want to use the Binder method described in Subsection 2.6.4. We take the Binder cumulant defined as

$$U_4 = \frac{\langle (\mathcal{M}_A^4 + \mathcal{M}_B^4) \rangle}{\langle (\mathcal{M}_A^2 + \mathcal{M}_B^2) \rangle^2} \tag{7.8}$$

for different lattice sizes, and calculate intersection points of consecutive lattice sizes with ratio 2. Note that we measure the Binder cumulant as described in Section 6.6. We have 8 intersection points which can be considered as pseudo-critical couplings $\tilde{p}_{L_i,2L_i}$ (see Figure 7.10). These pseudo-critical couplings are plotted as a function of $\frac{1}{L_{\text{min}}}$, where $L_{\text{min}} = \min\{L_i, 2L_i\} = L_i$. The size-dependent behavior of the pseudo-critical couplings can be described very well by fitting it as

$$ex^{\kappa} + p_{c,\text{Binder}}, \tag{7.9}$$

where $e, \kappa, p_{c,\text{Binder}}$ are fit parameters. The offset $p_{c,\text{Binder}}$ of the fit gives a prediction for the true critical coupling $p_c$ for $L \to \infty$, i.e., for infinite volume (see Figure 7.11).
For the 3 fit parameters we obtain

$$e = 0.048(2), \qquad \kappa = 0.44(3), \qquad p_{c,\text{Binder}} = 0.3576(5). \tag{7.10}$$

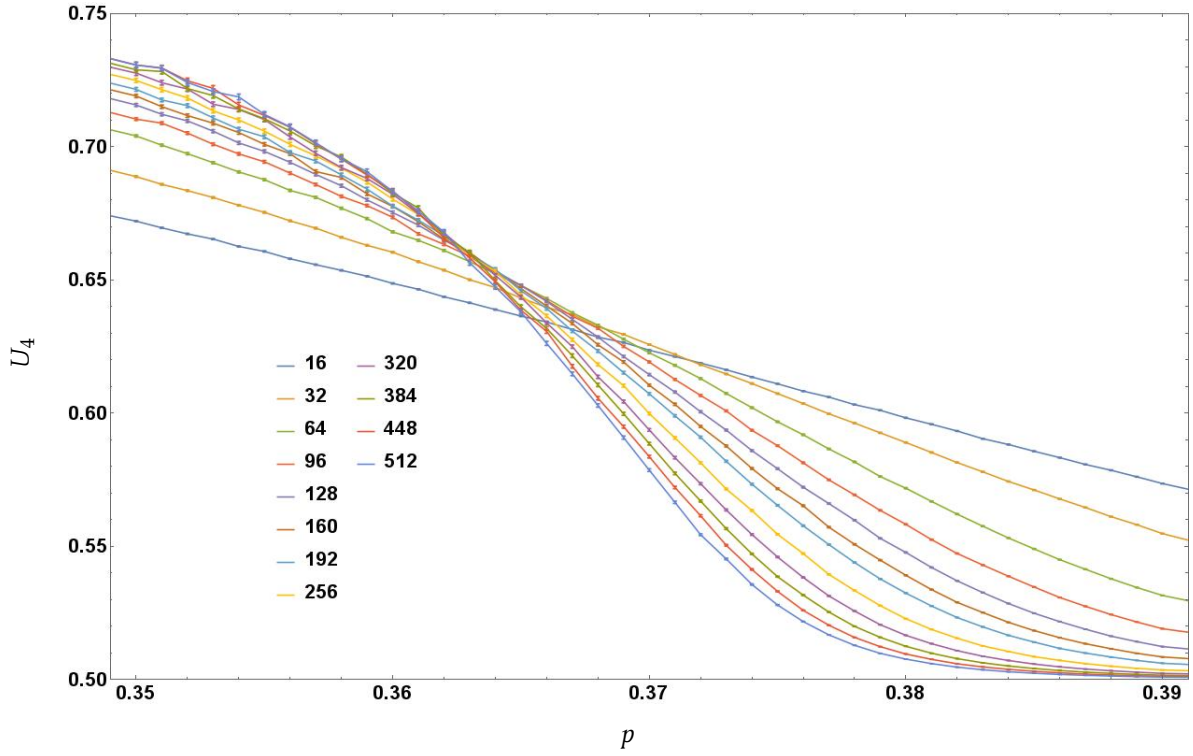


**Figure 7.10:** Binder cumulant for all different lattice sizes $L$.

## 7.5 Finite-Size Scaling Procedure

in Subsection 2.6.5 we discussed the classical two-dimensional XY model near its BKT-transition. We described the finite-size scaling ansatz for the susceptibility at the critical coupling and obtained

$$\chi \propto L^{2-\eta_c}(\log(L))^{-2r_e}, \tag{7.11}$$

where $\eta_c = \frac{1}{4}$ and $r_e = \frac{-1}{16}$. Having a first accurate estimate for the critical coupling $p_c$, we can check wheter the finite-size scaling ansatz in Equation (7.11) can be reproduced. We take the logarithm on both sides and substitute $x = \log(L)$ such that we obtain

$$\begin{aligned} \ln(\chi) &\sim (2-\eta)\ln(L) + (-2r_e)\ln(\ln(L)) + b \\ &\sim (2-\eta)x + (-2r_e)\ln(x) + b. \end{aligned} \tag{7.12}$$

The additional logarithmic correction means that $\ln(\chi)$ grows faster than $(2-\eta)x$, whereas the data on the contrary show a slower decrease. Fitting the data at $p_c = 0.3576$ and leaving the fit parameters $(\eta, r_e, b)$ free, leads to results

$$\eta = 0.2405(4), \qquad r_e = 0.0616(8), \tag{7.13}$$

which are not in agreement with the predicted behavior. Fixing $\eta_c$ or $r_e$ leads to big deviations in the other variable and also varying $p_c$ does not improve the fit by any means. The residues indicate that the form (7.11) is not the correct fit for $\chi$.
Balog predicted in [20, 21] that the true finite-size scaling behavior is

$$\begin{aligned} \ln(\chi) &\sim (2-\eta)x + \mathcal{O}(Q) + b \\ &\sim (2-\eta)x + a\frac{\frac{\pi^2}{2}}{(x+u)^2} + b, \end{aligned} \tag{7.14}$$

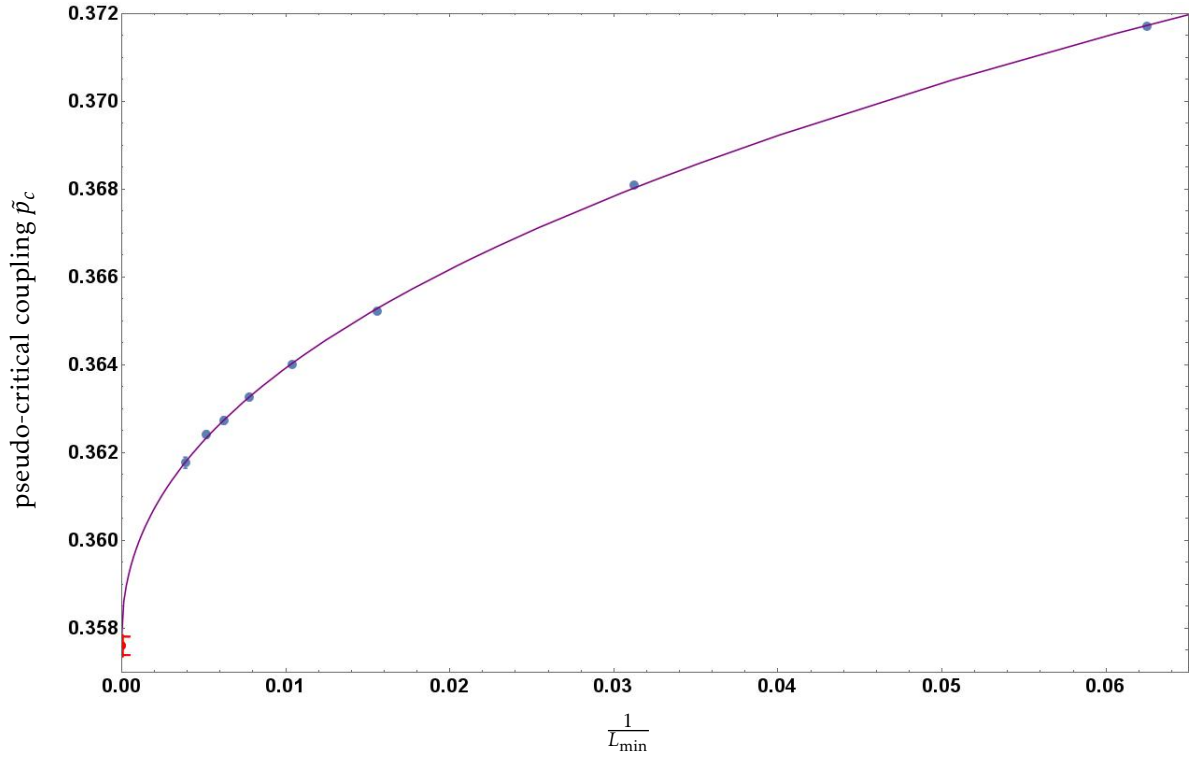


**Figure 7.11:** Pseudocritical couplings $\tilde{p}_c$, obtained by calculating intersection points of the Binder cumulants $U_4$. The offset of the fit is given by $p_{c,\text{Binder}} = 0.3576(5)$. Since the errors are very small the error bars are hardly visible.

at $p \approx p_c$, where $\eta, a, b$, and $u$ are fit parameters. Applying this fit to the data at $p = 0.3576$ we obtain

$$\eta = 0.247(3), \qquad a = 1.98(82), \qquad b = -0.29(4), \qquad u = 5.34(99). \tag{7.15}$$

The exponent $\eta$ is in agreement with the predicted critical exponent $\eta_c = 0.25$ and also the residues indicate that the correction term predicted by Balog is indeed correct. Fitting Equation (7.14) for the whole range $p \in [0,1]$ we realize that the correction term $Q$ comes into play when $p$ approaches $p_c$. Throughout the whole range $p \in [0,1]$ we obtain a continuously varying critical exponent $\eta = \eta(p)$, starting from $\eta \approx 1.00$, reaching $\eta_c = 0.25$ at the critical coupling $p_c$, and then rapidly decreasing to $\eta \approx 0$, for $p \to 1$. There is, however, an inconsistency for the range $p \in [0.36, 0.40]$ because the fitted values for $\eta$ become negative which is an unreasonable progression. The reason for this behavior is the divergence of the correction term $Q$ leading to additional contributions to the value of $\eta$. Applying a Taylor expansion for the correction term $Q$ at $x_0 = \frac{\ln(16)+\ln(512)}{2} \approx 4.505$, one obtains a correction term to the critical exponent $\eta$. The effective critical exponent $\eta_{\text{eff}}$ then reads

$$\eta_{\text{eff}} = \eta - Q'(x_0) = \eta + \frac{a\pi^2}{(x_0+u)^3}. \tag{7.16}$$

Plotting the progression of the critical exponent $\eta$ which results directly from the fit and the effective critical exponent $\eta_{\text{eff}}$, we see the coupling-dependent behavior of both exponents (see Figure 7.12).

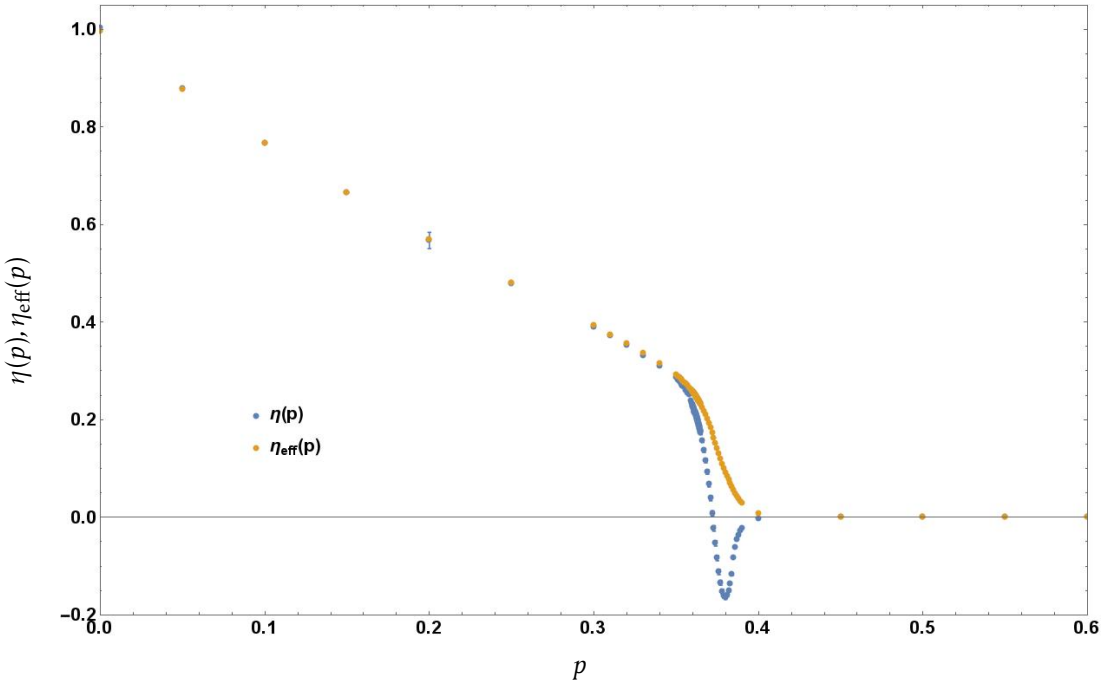


**Figure 7.12:** Progression of the critical exponent $\eta$. The correction term $Q$ leads to a large discrepancy between $\eta(p)$ and $\eta_{\text{eff}}(p)$.

## 7.6 Taylor Fit

Fitting the data for $\chi(L)$ (for fixed $p$) to the finite-size scaling ansatz (7.14) leads to large errors in the fit parameters $(\eta, a, b, u)$, since we are fitting a function with 4 parameters to 12 data points. We want to use the fact that $u$ is a non-universal constant, such that we can fix $u$ in the vicinity of the critical point and reduce the number of parameters to 3. Since the progression of all fit parameters $(\eta, a, b, u)$ is continuous and smooth in the neighborhood of $p_{c,\text{Binder}} \approx 0.3576$, we perform a Taylor expansion of the fit parameters around a hypothetical critical coupling $p_c$

$$\begin{aligned}
\eta(p) &= \eta_c + \eta_1(p - p_c) + \mathcal{O}((p - p_c)^2), \eta_c = \frac{1}{4}, \\
a(p) &= a_c + a_1(p - p_c) + \mathcal{O}((p - p_c)^2), \\
b(p) &= b_c + b_1(p - p_c) + \mathcal{O}((p - p_c)^2), \\
u(p) &= u_c.
\end{aligned}$$

Using this expansion we include several probabilities near the critical coupling $p_c$ and fit them altogether. For this fit we were using

$$p \in \{0.3560, 0.3561, \cdots, 0.3589, 0.3590\}, \tag{7.17}$$

which implies that we are using 372 data points in order to fit 7 parameters $(p_c, \eta_1, a_c, a_1, b_c, b_1, u_c)$. Using the Taylor fit expansion we obtain

$$\begin{aligned}
p_c &= 0.3579(1), & u_c &= 3.39(11), \\
\eta_c &= 0.25, & \eta_1 &= -5.00(5), \\
a_c &= 0.82(5), & a_1 &= 57(4), \\
b_c &= -0.238(3), & b_1 &= -14.43(42).
\end{aligned}$$

The result for the critical coupling $p_c$ differs slightly from the one obtained by using the Binder method, but both are still consistent with each other within their statistical errors

$$p_{c,\text{Binder}} = 0.3576(5) \qquad p_{c,\text{Balog Fit}} = 0.3579(1). \tag{7.18}$$

## 7.7 Helicity Modulus

In Subsection 2.6.5 we described the helicity modulus, which is defined in its dimensionless form as

$$\Upsilon = \frac{1}{T}\frac{\partial^2}{\partial \alpha^2} F(\alpha)\Big|_{\alpha=0}, \tag{7.19}$$

where $\alpha$ is the twist angle imposed at the boundary. The helicity modulus provides a measure for the spin stiffness of an XY model. By dualizing an XY model, we obtain a height model where the spin stiffness is described by the winding number squared $W_x^2$, i.e.,

$$\Upsilon = \langle W_x^2 \rangle. \tag{7.20}$$

Measuring $W_x^2$ for the $\tilde{F}_\Delta$ model, we recognize that we obtain similar numerical values for all the different lattice sizes we take into consideration. For the sake of clarity we only plot $\langle W_x^2 \rangle(p)$ for the lattice size $L = 512$.

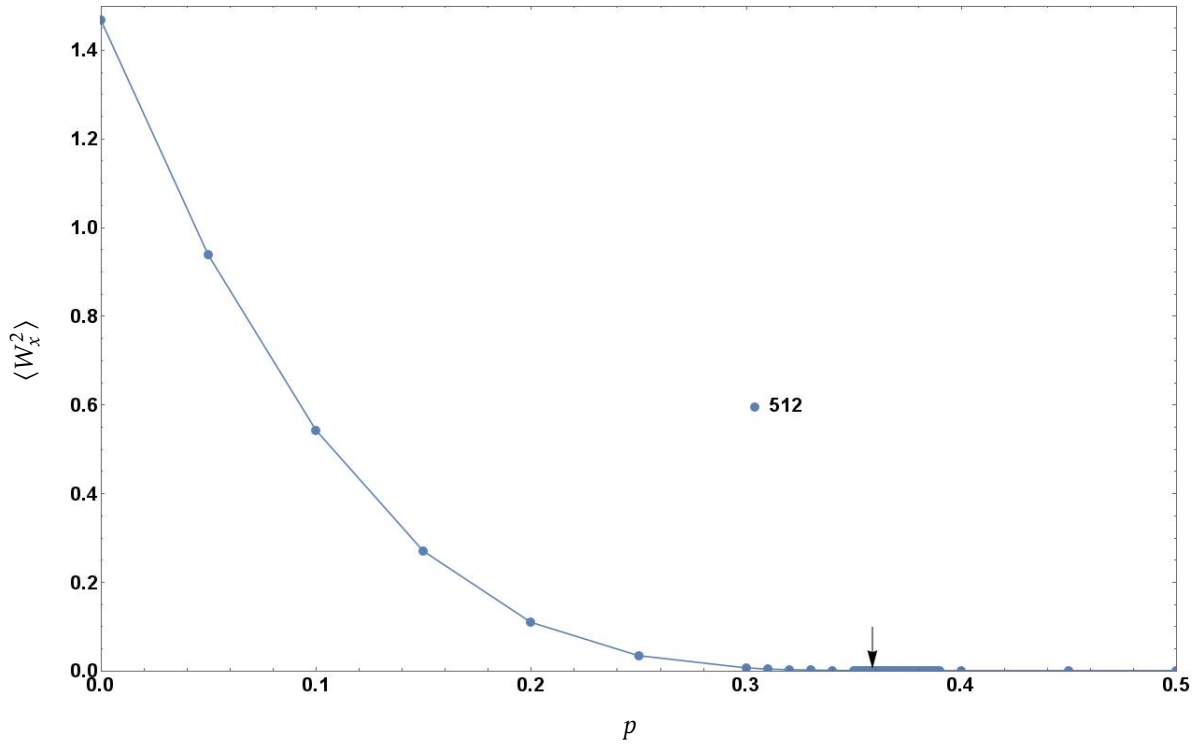


**Figure 7.13:** Winding number $\langle W_x^2 \rangle$, the arrow indicates $p_{c,\text{Binder}}$.

Compared to the predicted behavior in Figure 2.8, we see that we do not have a similar behavior for the winding number squared $\langle W_x^2 \rangle$. The reason for this is that we excluded certain configurations described in Subsection 6.1.2, since we are only able to sample a certain number of winding sectors (namely the ones where $W_x \mod 4 = 0$ and $W_y \mod 4 = 0$). Nonetheless, we also see that the winding number $\langle W_x^2 \rangle$ is decreasing rapidly and approaches 0 around $p \approx p_c$. However, no universal jump has been determined.

# 8 Summary and Interpretation of the Results

Now we want to briefly discuss our results and put them into context with the classical XY model and its BKT-transition (compare with Figure 2.7). We simulated the $\tilde{F}_\Delta$ model, where we first applied the modulo 4 formulation and then mapped this formulation to an Ising-type model in order to measure observables. The magnetization of both sublattices $(\mathcal{M}_A, \mathcal{M}_B)$, the susceptibility $\chi$, and the absolute value of the magnetization per spin $|\mathcal{M}|_{\text{p.s.}}$ reveal a phase transition to a rigid phase, that takes place at a certain critical coupling. Measuring the correlation function $\Gamma(r)$ for $p \in [0,1]$ reveals that for $p \in [0, p_c]$ it behaves as $\Gamma(r) \propto \frac{1}{r^{\eta}}$, with a continuously varying critical exponent $\eta = \eta(p)$. For $p \in (p_c, 1]$ we enter a rigid phase where infinite correlations arise and $\Gamma(r) \propto 1$. This shows that the phase transition we are dealing with is a dual form of a BKT-transition, separating a rough phase for $p \in [0, p_c]$ from an rigid one for $p \in (p_c, 1]$. The Binder cumulant provided a first precise estimate of the critical coupling $p_{c,\text{Binder}}$. Fitting our data for the susceptibility $\chi = \chi(L, p = \text{fixed})$ to the finite-size scaling prediction by Balog did not only confirm our previous result for $p_{c,\text{Binder}}$, but also confirmed that the exponent $\eta$ at the critical point is indeed given by $\eta_c = \eta(p_c) = \frac{1}{4}$. The connection to the classical XY model can be made by dualizing the $\tilde{F}_\Delta$ model. The analogue of Figure 2.7 in our case is similar but flipped (see Figure 8.1).

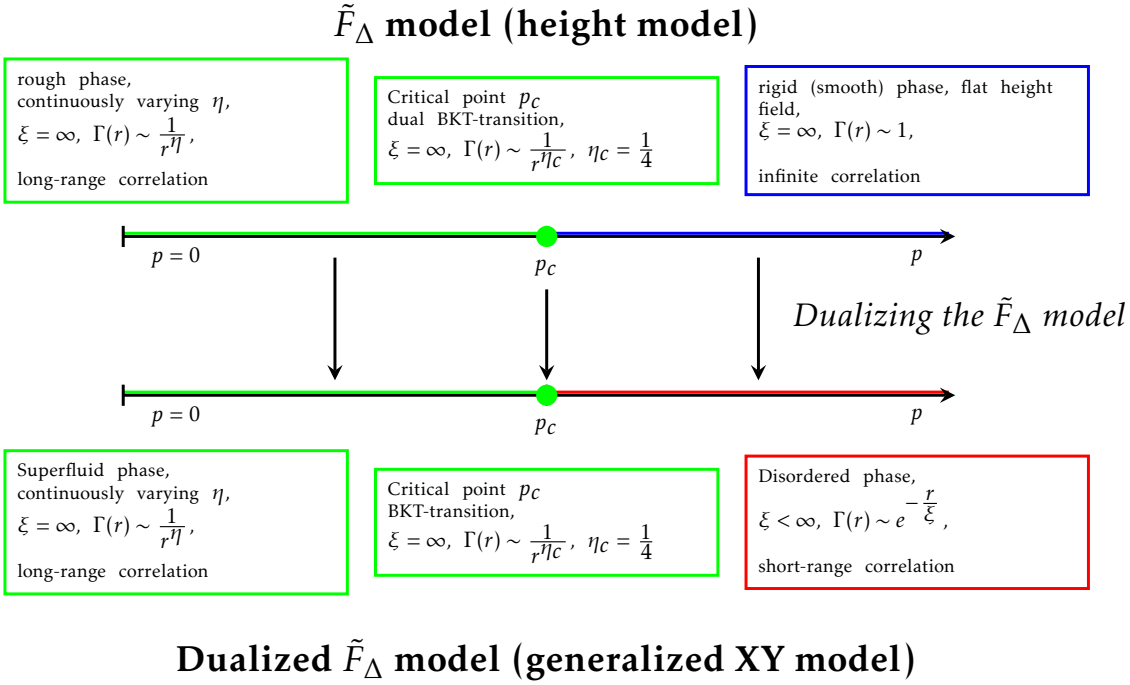


**Figure 8.1:** $\tilde{F}_\Delta$ model with dual BKT-transition.

# 9 Conclusion and Outlook

In this thesis we investigated the $\tilde{F}_\Delta$ model on a honeycomb lattice, which was mentioned by Prof. Martin Hairer in 2016 at his Einstein lectures at the university of Bern. This model belongs to the class of height models and constrains nearest-neighboring height variables to differ by $\pm 1$. We used the methods of the dual transformation and the star-triangle transformation to obtain the dualized $\tilde{F}_\Delta$ model on a honeycomb lattice, which belongs to the class of two-dimensional $U(1)$ models and has a severe sign problem which prevents numerical simulations. Therefore we simulated the original $\tilde{F}_\Delta$ model, by using a modulo 4 formulation.
Studying the correlation function and the susceptibility revealed a dual BKT-transition at a critical coupling $p_c$. Using the Binder method, we obtained a reliable result for the critical coupling $p_c$, which was confirmed by combining the finite-size scaling ansatz proposed by Balog with a Taylor fit around the critical point. We obtained the following results

$$p_{c,\text{Binder}} = 0.3576(5) \qquad\qquad p_{c,\text{Balog Fit}} = 0.3579(1).$$

Still there are open questions one would like to address. Is it possible to perform a dual transformation (section 5.3) without setting the coupling parameter $K$ to zero? If so, is it possible to analytically derive the critical coupling? Can one construct an algorithm which allows us to dynamically enter winding sectors we could not reach before (subsection 6.1.2)? If so, is it possible to compare the behavior of $\langle W_x^2 \rangle$ with the behavior of the helicity modulus $\Upsilon$, and check its universal jump at the BKT transition?
The $\tilde{F}_\Delta$ model is an interesting height model which allows generalizations and leaves open questions. In this thesis we have laid the groundwork for potential future studies.

**Acknowledgement**

It is a pleasure to thank Uwe-Jens Wiese for introducing me to this interesting topic, for his advice and patience throughout the last year. Special thanks go also to Stephan Caspar. He assisted me in a variety of different tasks and always had an answer at hand when I got stuck in a problem.

# A Formulas

## A.1 Fourier Representation

If $b(k)$ is a function of some integer $k \in \mathbb{Z}$, it can be represented as the integral of a $2\pi$-periodic function $f_{2\pi}$, such that

$$b(k) = \frac{1}{2\pi} \int_0^{2\pi} e^{-ik\varphi} f_{2\pi}(\varphi) \mathrm{d}\varphi, \tag{A.1}$$

and

$$f_{2\pi}(\varphi) = \sum_{q \in \mathbb{Z}} b(q) e^{iq\varphi}. \tag{A.2}$$

## A.2 Dirac Comb

In order to evaluate certain sums that arise in the dualization procedure we used the Dirac comb, which is a periodic tempered distribution constructed from Dirac-Delta-functions

$$\delta_T(t) \overset{\text{def.}}{=} \sum_{k \in \mathbb{Z}} \delta(t - kT) = \frac{1}{T} \delta_T(\frac{t}{T}), \tag{A.3}$$

for some given period $T$. Due to $T$-periodicity, the Dirac comb can be expressed as a Fourier expansion

$$\delta_T(t) = \sum_{n \in \mathbb{Z}} b(n) e^{2\pi i n \frac{t}{T}} = \frac{1}{T} \sum_{n \in \mathbb{Z}} e^{2\pi i n \frac{t}{T}}, \tag{A.4}$$

where $b(n)$ is given by

$$b(n) = \frac{1}{T} \int_{-\frac{T}{2}}^{\frac{T}{2}} \delta_T(t) e^{-2\pi i n \frac{t}{T}} \mathrm{d}t = \frac{1}{T}. \tag{A.5}$$

## A.3 Poisson Summation Formula

The Poisson summation formula reads

$$\sum_{\mu \in \mathbb{Z}} g(\mu) = \sum_{n \in \mathbb{Z}} \int_{\mathbb{R}} e^{2\pi i n \phi} g(\phi) \mathrm{d}\phi. \tag{A.6}$$

This identity is true for any function $g(x)$, which is analytical for real values of $x$ and for which the integral

$$\int_{\mathbb{R}} e^{2\pi i n \phi} g(\phi) \mathrm{d}\phi \tag{A.7}$$

is absolutely convergent.

# Bibliography


[1] M. Hasenbusch, G. Lana, M. Marcu, and K. Pinn. Cluster algorithm for a solid-on-solid model with constraints. *Phys. Rev. B*, 46(16):10472, 1992.

[2] K. Binder and D. P. Landau. *A Guide to Monte Carlo Simulations in Statistical Physics*. Cambridge University Press, 2 edition, 2000.

[3] A. Wipf. *Statistical Approach to Quantum Field Theory*. Springer, 2013.

[4] R. B. Potts. Some generalized order-disorder transformations. *Proc. Camb. Philos. Soc.*, 48(106), 1952.

[5] G. H. Wannier and H. A. Kramers. Statistics of the two-dimensional ferromagnet. part i. *Phys. Rev.*, 60:252, 1941.

[6] G. H. Wannier. The statistical problem in cooperative phenomena. *Rev. Mod. Phys.*, 17:50, 1945.

[7] P. Serna, J. T. Chalker, and P. Fendley. Deconfinement transitions in a generalised XY model. *J. Phys. A*, 50, 2017.

[8] D. H. Lee and G. Grinstein. Strings on two-dimensional classical XY models. *Phys. Rev. Lett.*, 55:541, 1985.

[9] S. E. Korshunov. Possible splitting of a phase transition in a 2d XY model. *JETP*, 41:263, 1985.

[10] R. J. Baxter. F model on a triangular lattice. *J. Math. Phys.*, 10:1211, 1969.

[11] H. Wagner and N. D. Mermin. Absence of ferromagnetism or antiferromagnetism in one- or two-dimensional isotropic Heisenberg models. *Phys. Rev. Lett.*, 17:1133, 1966.

[12] P. C. Hohenberg. Existence of long-range order in one and two dimensions. *Phys. Rev.*, 158:383, 1967.

[13] M. E. Fisher. *Critical Phenomena*. Academic Press London, 1971.

[14] V. Privman. *Finite Size Scaling and Numerical Simulation of Statistical Systems*. World Scientific, Singapore, 1990.

[15] K. Binder. *Computational Methods in Field Theory*. Springer, 1992.

[16] K. Binder. Finite size scaling analysis of Ising model block distribution functions. *Zeitschrift fuer Physik*, B43:119, 1981.

[17] J. M. Kosterlitz. The critical properties of the two-dimensional XY model. *J. Phys. C: Solid State Phys.*, 7:1046, 1974.

[18] R. Kenna. The XY model and the Berezinskii-Kosterlitz-Thouless phase transition. "`http://www.mariecurie.org/~mariecur/annals/volume4/phy4.pdf`".

[19] M. Hasenbusch. The two-dimensional XY model at the transition temperature: a high-precision Monte Carlo study. *J. Phys. A: Math. Gen.*, 38:5869, 2005.

[20] J. Balog. Kosterlitz-Thouless theory and lattice artifacts. *J. Phys. A: Math. Gen.*, 34:5237, 2001.

[21] J. Balog, M. Niedermaier, F. Niedermeyer, A. Patrascioiu, E. Seiler, and P. Weisz. Does the XY model have an integrable continuum limit? "https://arxiv.org/abs/hep-lat/0106015v3", December 2006.

[22] M. Hasenbusch. The Binder cumulant at the Kosterlitz-Thouless transition. *J. Stat. Mech.*, 2008.

[23] U. Gerber and W. Bietenholz. Berezinskii-Kosterlitz-Thouless transition and the Haldane conjecture: Highlights of the physics Nobel prize 2016. "https://arxiv.org/abs/1612.06132", 2017.

[24] U.-J. Wiese. Sign and complex action problems: The Potts model approximation to dense QCD as a solvable example. "http://www.wiese.itp.unibe.ch/lectures/sign.pdf", 2006.

[25] L. Onsager. Crystal statistics. i. A two-dimensional model with an order-disorder transition. *Phys. Rev.*, 65:117, 1944.

[26] C. Domb and M. S. Green. *Phase Transitions and Critical Phenomena*. 1. Academic Press London, 1972.

[27] A. McIntosh. The Jackknife estimation method. "https://arxiv.org/abs/1606.00497".

**Selbstständigkeitserklärung**

gemäss Art. 28 Abs. 2 RSL 05

Name/Vorname: Bühlmann Patrick

Matrikelnummer: 13-101-126

Studiengang: Master of Science in Physics
Bachelor ☐ Master ☒ Dissertation ☐

Titel der Arbeit: Height Models on a Honeycomb Lattice
Leiter der Arbeit: Prof. Dr. U.-J. Wiese

Ich erkläre hiermit, dass ich diese Arbeit selbständig verfasst und keine anderen als die angegebenen Quellen benutzt habe. Alle Stellen, die wörtlich oder sinngemäss aus Quellen entnommen wurden, habe ich als solche gekennzeichnet. Mir ist bekannt, dass andernfalls der Senat gemäss Artikel 36 Absatz 1 Buchstabe r des Gesetzes vom 5. September 1996 über die Universität zum Entzug des auf Grund dieser Arbeit verliehenen Titels berechtigt ist. Ich gewähre hiermit Einsicht in diese Arbeit.

Datum/Ort: 25. April 2018
3012 Bern

Unterschrift:

Bühlmann Patrick